Acoustic Trapping in Biomedical Research

Hammarström, Björn

2014

Acoustic Trapping in Biomedical Research

Björn Hammarström

LUND
UNIVERSITY

DOCTORAL DISSERTATION

by due permission of the Faculty of Engineering, LTH, Lund University, Sweden.

To be defended at E:1406, E-building, Ole Römers väg 3, Lund. 23 May 2014 at 10:15.

Faculty opponent

Martin Viklund

Organization LUND UNIVERSITY Department of Biomedical Engineering P.O. Box 118, SE-221 00 Lund, Sweden	**Document name** DOCTORAL DISSERATION **Date of issue:** 23 May, 2014
Author Björn Hammarström	**Sponsoring organizations** Swedish Research Council, The Crafoord Foundation, Knut och Allice Wallenberg, Sigfrid och Walborg Nordkvist, Kungliga Fysiografiska Sällskapet

Title: Acoustic Trapping in Biomedical Research

Abstract

Herein a method that uses acoustically resonating glass capillaries and enables non-contact capture of micron-sized bioparticles, i.e. acoustic trapping, is described. A miniaturized ultrasonic transducer is used to locally actuate a cross-sectional resonance in the capillary. A 2000×200 μm^2 capillary is typically operated around a resonance frequency of 4-MHz. Optimal design of the transducer for this purpose is investigated in detail, showing that mode-control in the transducer results in a more efficient device, and makes automatic frequency tracking possible. A system design that allows easy assembly and disassembly of the transducer and the capillary also demonstrates how a single-use device can be accomplished.

A breakthrough for the presented acoustic trapping technology is the introduction of seed-particles. These enable trapping of submicron particles that would otherwise be impossible to capture in this kind of system. It is shown how controlled interaction with the larger seed particles can circumvent this limitation. Using this approach capture of 110 nm particles and Escherichia coli bacteria is demonstrated with 95% capture efficiency.

The usefulness of the acoustic trapping device in biomedical research is demonstrated in applications such as; efficient washing of functionalised beads for biomarker detection in blood plasma, dynamic studies of cell-drug interactions, and purification and identification of microbes from infected blood. To enable these applications the acoustic trap an interface to a Matrix Assisted Laser Desorption/Ionization Mass Spectrometry (MALDI MS) instrument has been devised. This is facilitated by designing the acoustic trap to operate in aspirate/dispense mode (like a pipette) depositing liquids in a microchip for solid phase extraction and subsequent MALDI MS analysis.

Tracking and logging the system resonance frequency provides a new way to measure the amount of captured material as well as continuously adjusting the driving frequency to changes in the infused samples. Apart from providing a new measurement method, continuously adapting the resonance frequency enables samples with a wider range of acoustic properties to be processed. This is demonstrated in an assay for bacteria typing with MALDI MS in blood cultures. Here, acoustic trapping provides a faster and more automatable sample preparation method as compared to the one currently used in the clinical assay.

Key words: Acoustic Trapping, Ultrasound, Microfluidics, Lab-on-a-Chip, Mass Spectrometry

Classification system and/or index terms

Supplementary bibliographical information **Language:** English

ISRN: LUTEDX/TEEM – 1094 – SE, Report 1/14

ISSN and key title	**ISBN** 978-91-7473-989-3 (Print) 978-91-7473-990-9 (Electronic)
Recipient's notes	**Number of pages:** 70 **Price** **Security classification**

Signature _____ Date _____

Acoustic Trapping in Biomedical Research

Björn Hammarström

LUND
UNIVERSITY

Department of Biomedical Engineering
Faculty of Engineering

ISBN 978-91-7473-989-3 (Print)
ISBN 978-91-7473-990-9 (Electronic)
ISRN LUTEDX/TEEM – 1094 – SE, Report 1/14

Lund 2014

Table of contents

List of papers

Included

Paper I

Non-Contact Acoustic Cell Trapping in Disposable Glass Capillaries

B. Hammarström, M. Evander, H. Barbeau, M. Bruzelius, J. Larsson, T. Laurell, and J. Nilsson

Lab on a Chip, 2010, 10 (17), 2251-2257.

Author contribution: All simulations; major part of system design, data analysis, and writing; large part of experimental.

Paper II

Seed Particle-Enabled Acoustic Trapping of Bacteria and Nanoparticles in Continuous Flow Systems

B. Hammarström, T. Laurell, and J. Nilsson

Lab on a Chip, 2012, 12 (21), 4296-4304.

Author contribution: All experimental, and system design; major part of data analysis, and writing.

Paper III

Efficient Sample Preparation in Immuno-Matrix-Assisted Laser Desorption/Ionization Mass Spectrometry using Acoustic Trapping

B. Hammarström, H. Yan, J. Nilsson, and S. Ekström

Biomicrofluidics, 2013, 7 (2), 024107.

Author contribution: Major part of system design, experimental, and writing; large part of data analysis.

Paper IV

Frequency Tracking in Acoustic Trapping for Improved Performance Stability and System Surveillance

B. Hammarström, M. Evander, J. Wahlström, and J. Nilsson

Lab on a Chip, 2014, 14 (5), 1005-1013.

Author contribution: Major part of system design, experimental, data analysis, and writing.

Paper V

Acoustic Trapping for Bacteria Typing in Blood Culture with MALDI MS

B. Hammarström, B. Nilson, T. Laurell, J. Nilsson, and S. Ekström

Manuscript

Author contribution: Major part of system design, experimental, and data analysis; large part of writing.

Related

Paper VI

Review of Cell and Particle Trapping in Microfluidic Systems,

J. Nilsson, M. Evander, B. Hammarström, T. Laurell

Analytica Chimica Acta, 2009, 649, 2, 141-157.

Author contribution: Reference study and writing for chapter on acoustic trapping.

1 Introduction to trapping in biomedical research

1.1 Trapping in biomedical research

New understanding of biology has often been closely linked to technological developments. There are numerous examples of this interconnectivity, ranging from the invention of the microscope that allowed discovery of microorganisms [1], to modern technology that enables low-cost complete genome sequencing [2, 3]. An example that is somewhat related to the acoustic cell trap presented herein is the patch-clamp technique [4, 5], that was awarded the Nobel Prize in Physiology or Medicine in 1991. Essentially, it is a micro-pipetting technique that allows capture of a single cell and study of its membrane potential – an invention that allowed novel insights about the workings of ion-channels in the cell membrane.

Manufacturing techniques from micro- and nanotechnology allow conventional processes for chemical or biological analysis to be scaled-down in so called μTAS or lab-on-a-chip devices [6]. The key feature in such devices is the microfluidic format that allows miniaturization and automation of biological assays [7]. Here, the miniaturized format enables fast reactions and low sample consumption [8], and integration of several assay steps in the same chip can allow automation of complex assays [9, 10]. Trapping (i.e. capture and retention) of biological particles is a useful function in such systems as it allows enrichment in a small volume, and the sequential treatment of retained particles for automation of multiple assay steps. A challenge with the lab-on-a-chip approach is the diversity of different assays found in biomedical research. When automation and integration are prioritized the trade-off is flexibility, therefore each individual applications often require development of new specially tailored devices. For the lab-on-a-chip approach to be efficient the microfluidic devices must be either designed to perform unit operations that can be integrated with other devices, or there has to be a strong need to perform the same assay over and over again. One example of the latter situation is clinical laboratory diagnosis[11, 12] where routine assays are performed repeatedly on new patients and it is critical to obtain a reliable, operator-independent, and fast readout.

Biological particles that would be of interest to subject to trapping vary greatly in size. **Figure 1** compares the size intervals for particles ranging from micron sized eukaryotic cells to nanometer sized proteins.

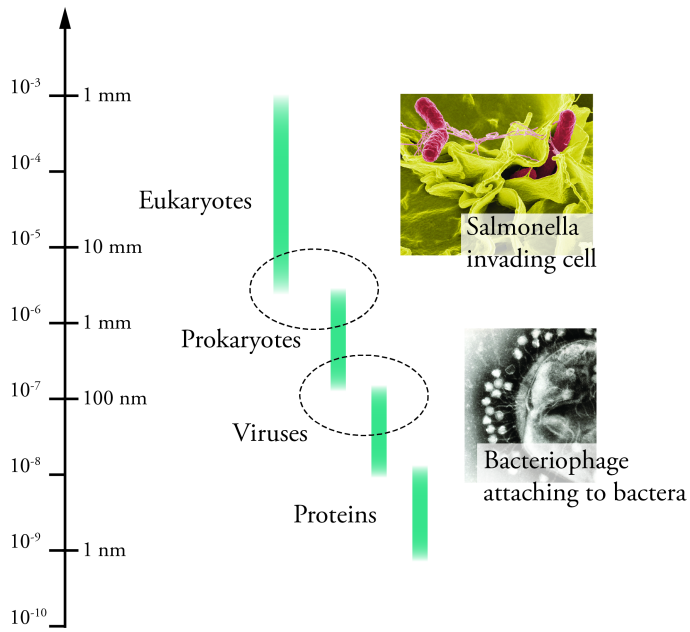

Figure 1: Size intervals for some important classes of biological particles, and two tentative images with particle interactions at the micro- and the nanoscale.
The electron micrograph insets are adapted from Wikimedia commons public domain [13, 14].

From a measurement perspective the study of biological particles provide some unconventional challenges. In the classical sense the quality of a measurement can be determined by its sensitivity and specificity. However, when studying living organisms their behaviour will be strongly influenced by environment. Therefore the relevance of the measurement must also be questioned. There can in fact be a significant gap between the behaviour in a test system (*in vitro*) and in its natural environment (*in vivo*) [15]. For instance, in the development of new pharmaceuticals this gap can incur great costs when promising drug candidates selected from *in vitro* tests fail when applied *in vivo* as part of a complex biological system [16]. In this context, microfluidics combined with non-contact particle handling has potential to improve the used model system in question by providing precise control of the microenvironment [17].

When studying biological particles at micro- or nano-scale our understanding of the particles is very much determined by what we can measure. In microfluidic systems as well as in, fluorescence activated cell sorters (FACS-machines) and microtitre plate-based assays optical readouts utilizing antibodies and fluorescent labels are widely used. This type of readout typically provides a sensitive detection that is readily integrated with microfluidics. There are, however, circumstances where a label-free readout may be preferred. One example is the study of receptor-ligand interaction. Here, the attachment of a fluorescent probe, which can sometimes be as large as the ligand itself, may raise questions as to whether a relevant interaction is observed. In contrast, a mass-spectrometric readout can be obtained without utilizing fluorescent labels or antibodies, providing first-hand information about the analytes. Another major advantage is the possibility to study multiple analytes

simultaneously. A recent example that illustrates this is the use of matrix-assisted laser desorption/ionization mass spectrometry (MALDI MS) for typing of bacteria [18]. Here, a database with a characteristic spectrum for each species is compared to the spectra obtained from the sample providing a robust identification method based on several peaks in the mass spectrum.

While potential benefits exist, some practical challenges occur when integrating a lab-on-a-chip device with mass spectrometry. Firstly the decreased sensitivity (as compared to fluorescence) may become a problem if the sample volume is too small, and secondly the samples have to be extracted from the chip for analysis. This seemingly simple extraction is a challenge for complex systems, as the small sample volume may suffer from dispersion when pumped through microchannels or tubing. In this thesis, providing a practical solution for integration of acoustic trapping and MALDI MS readout has been an important aspect.

1.2 Micro-particle capture technologies

Several technologies for capture and retention of cells and microparticles have been demonstrated in a microfluidic setting (Paper VI). Based on the capture mechanism these can be classified into either hydrodynamic, optical, dielectrophoretic, magnetic, or acoustic. Comparison of these modalities is important as it allows the best-suited technology to be pinpointed based on the demands set by each application.

A desired feature is often non-contact operation, i.e. allowing capture and retention of cells without surface contact. Non-contact trapping has practical advantages such as a decreased risk of clogging if the trap is overloaded, and minimal loss of particles due to sticking to surfaces. This is primarily important for sample preparation application such as enrichment and purification of cells. In other cases, such as when attempting functional studies of non-adherent cells, there are important conceptual advantages as surface contact can be considered a perturbation for such cells. Furthermore, chemical approaches for attaching cells to surfaces [19, 20] and long-since developed mechanical filters provide stiff competition for contact trapping.

To make fair comparisons of trapping technologies there are multiple aspects to consider. Different technologies have different discriminating parameters; these are physical properties of the particles that in turn determine the trapping force. For most technologies the particle size is a discriminating parameter making small particles increasingly difficult to capture. The forces may also be dependent on the buffer, thereby restricting buffers that can be used and in turn the suitable applications. While the magnitude of the trapping force is perhaps the most important feature it is typically determined by many factors making comparisons approximate. For some applications, such as high-resolution microscopy, the spatial resolution of the trap can also be important. However, spatial resolution can often come at the cost of trapping capacity, i.e. the number of particles that can be captured, as this requires distributing forces over a larger area. While no standardized benchmarking

system for trapping technologies has yet been adopted, a comparison of published parameters is provided in **Table 1**.

Table 1: A general comparison of trapping modalities is useful when considering the best technology for a specific application. The trapping force magnitudes are taken from the literature in the given references.

Trapping Technology	Hydrodynamic	Optical	Dielectrophoretic	Magnetic	Acoustic
Discriminating parameters	D	D, n	D, ε, σ	D, χ	D, ρ, β
Buffer demands		Transparent	pH, ion, clean surfaces		
System complexity (non-contact)	Low	High/Medium	Medium	High	Low
System complexity (contact)	Low	Scarcely operated in contact mode	Low	Low	Scarcely operated in contact mode
Trapping resolution	Low (~ 10 μm)	High (~ 50 nm)	Medium (~ 1μm)	Medium (~ 1 μm)	Low (~ 100 μm)
Singe cell trapping	Low	High	Medium	Medium	Low
Cell cluster trapping	Medium	Low	Medium	High	High
Trapping force / pN	NA	100 – 2000**	200-400	2 – 1000*	100 – 400
Force references		21-23	24, 25	26-35	36-39

Optical tweezers

Optical tweezers is perhaps the most well-known trapping modality. It was discovered by Arthur Ashkin [40] and was originally referred to as optical trapping. It is now developed far enough to be commercially available as an add-on for advanced microscopes. Optical tweezers uses a focused laser-beam to pinpoint single particles to specific positions [23]. This technology has an unparalleled spatial accuracy, as demonstrated in the molecular knot experiment [41] allowing the images in **Figure 2** to be taken. By attaching an actin filament to two microbeads each controlled by an optical trap the authors were able to tie a single-molecule knot. The optical trap is not necessarily limited to a single particle as demonstrated by holographic optical tweezers allowing particles to be distributed in a potential landscape created through optical interference [42]. While ideally suited for detailed single cell studies optical trapping utilizes a relatively complex optical setup that is hard to scale into a low cost parallelized system.

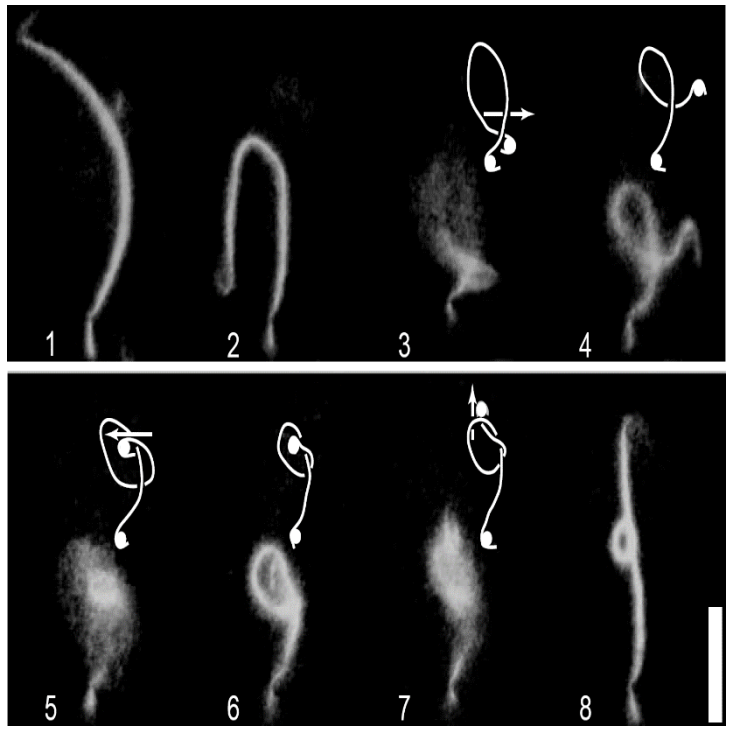

Figure 2: The high resolution of optical tweezers makes it possible to tie a molecular-knot on an actin filament, as demonstrated by attaching both ends of the filament to microbeads and using dual-beam optical tweezers (scale bar is 10 μm).
Reprinted by permission from Macmillan Publishers Ltd: Nature (Y. Arai, et al., Nature 399 (6735), 446-448 (1999)), copyright (1999).

Dielectrophoretic trapping

Dielectrophoretic trapping captures particles based on their complex permittivity and size. This phenomenon was described by Pohl in 1951 [43]. In contrast to electrophoresis, dielectrophoresis does not require charged particles but does require a non-uniform electric field [44]. To generate the sharp field gradients that enable dielectrophoretic trapping of small particles microscale device-features are key. Therefore, microfabrication plays a major role in fabricating effective dielectrophoresis-based traps. Two examples of successful dielectrophoresis devices are; the use of ring electrodes to create individually addressable trapping sites [25], and the use of an array of insulating posts [45], **Figure 3**. Although the insulator-based approach is not a non-contact technique it is an intriguing design as it provides a very scalable device.

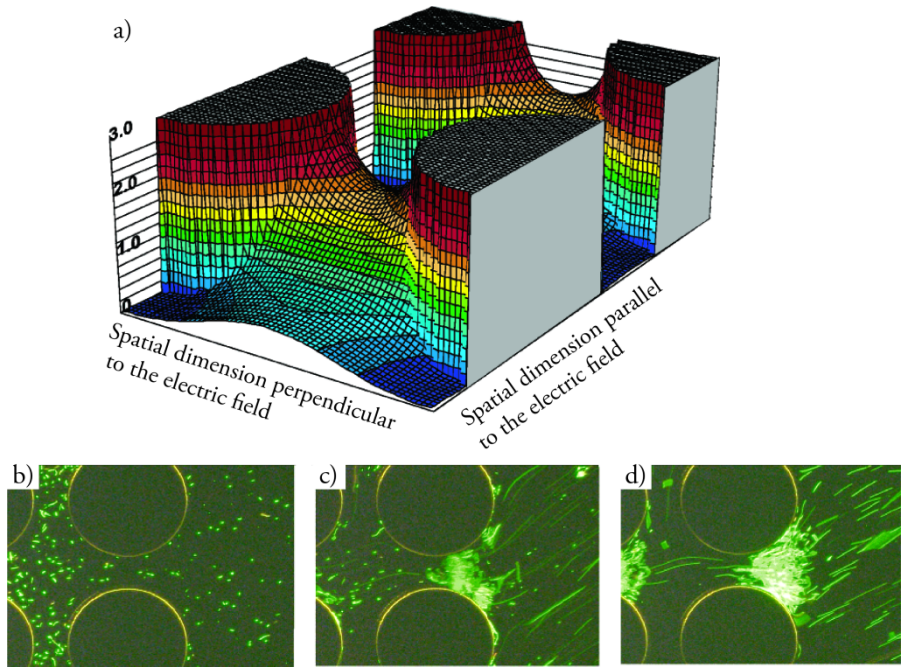

Figure 3: In insulator-based dielectrophoretic trapping a non-uniform electric field is created by the insulator posts. The normalized intensity in the simulation (a) shows how the field gradient allows Escherichia coli captured in the sequentially taken photos (b-d)
Adapted with permission from (B. H. Lapizco-Encinas, et al., Anal Chem 76 (6), 1571-1579 (2004)). Copyright (2004) American Chemical Society.

Magnetic trapping

In biomedical research the use of magnetic microparticles is widespread, such as the use of antibody-coated particles for protein enrichment or usage in a magnetic-activated cell sorter (MACS). The discriminating parameters for magnetic trapping are susceptibility and size. As living cells do not have suitable magnetic properties for this modality it is only suitable manipulation of specially engineered microparticles. On the other hand, the commercial success of magnetic-based particle manipulation clearly shows how many applications that can be addressed by the use of functionalized microparticles, and is therefore included in the comparison in **Table 1**.

Hydrodynamic trapping

Hydrodynamic trapping is fundamentally different from the other technologies, as it does not utilize an external field for particle capture. The precise control of flow enabled by microfluidic devices has provided the necessary prerequisites for variety of ingenious methods to be explored [46]. Many of the hydrodynamic techniques are contact mode techniques where cells are pushed against a small pore [47, 48]. However, examples of non-contact trapping exist such as the hydrodynamic tweezers shown in **Figure 4** where an oscillating flow is used to trap particles in the vicinity of a solid post in the channel [49, 50]. A minimalistic approach to of non-contact hydrodynamic trapping is to utilize two opposing

flows in a 4-way junction [51, 52]. This can create a trapping site in the centre of the junction, similar to how a ball can be trapped on top of a garden hose spraying water vertically. The most intriguing aspect of hydrodynamic trapping is the absence of a conventional trapping force. This means that for some designs flow could potentially be increased up to the limit of laminar flow regime. Drawbacks with hydrodynamic trapping are that it limits the freedom to control the fluidics separately, and that it for some applications can be beneficial to allow capture based on other properties than size.

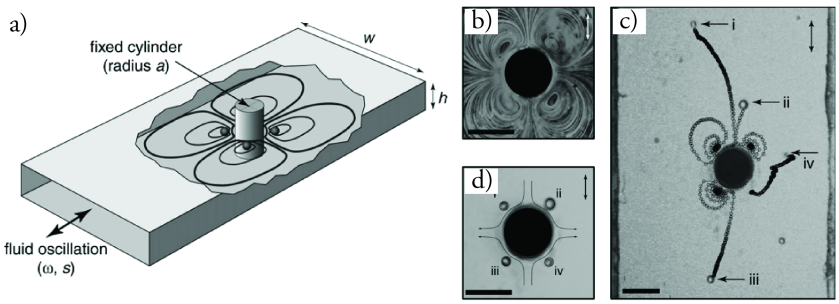

Figure 4: Non-contact hydrodynamic trapping in micro-vortices can be accomplished by using a solid post and an oscillating flow (a). This situation creates four micro-vortices (b) wherein particles travel along the streamlines (c) until reaching a stationary position (d).
Adapted with permission from (B. R. Lutz, et al., Anal Chem 78 (15), 5429-5435 (2006)). Copyright (2006) American Chemical Society.

Acoustic trapping

Acoustic trapping uses mechanical waves to manipulate particles, and the discriminating parameters are density and compressibility, these mechanisms are discussed in Section 2. A large variety of acoustic trapping devices will be considered in Section 1.3. For convenience a principal sketch of the acoustic trapping device used in this thesis is provided, in **Figure 5**, but will be discussed in greater detail in Section 3.

When comparing acoustic trapping to optical tweezers (**Table 1**) it is quite clear that optical trapping has far better resolution. This is expected as the wavelength of an optical wave is so much smaller than an acoustic. On the other hand, a long wavelength can be an advantage in that it allows capture of large groups of particles. For instance the device used in this thesis allows capture of approximately half a million 3 μm beads in a single site (Paper III). A high trapping capacity is primarily useful in sample preparation applications such as enrichment or washing. In contrast to applications such as single cell studies, in sample preparation it is typically useful to process large numbers of cells or particles. Furthermore, a large trapping capacity is useful when integrating the trap to a label-free mass spectrometric readout, as larger number of cells will compensate for lower sensitivity of mass spectrometry compared to optical read-out methods.

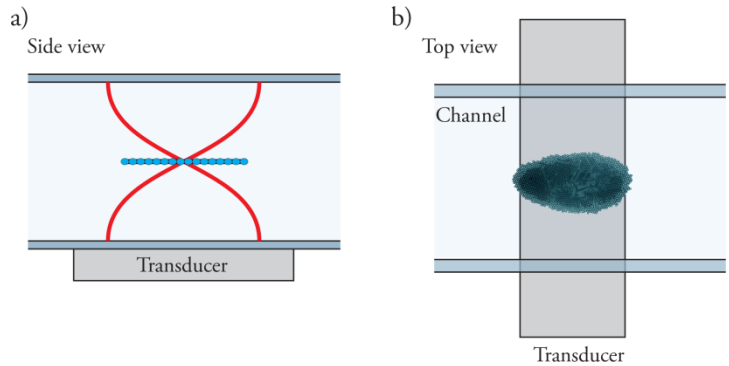

Figure 5: An ultrasonic standing wave is formed in a microfluidic channel pushing the particles towards the pressure node (a). The width of the ultrasonic transducer, actuating the resonance, defines the size of the acoustic trap and retains the particles above the transducer (b).

1.3 The development of acoustic trapping

Historical references

The fact that acoustic waves can exert forces on small particles was discovered during a famous experiment by August Kundt in [53], and originally presented as a way to measure the speed of sound in gaseous media. More than one hundred years later in1971 this effect was observed for biological particles in a liquid medium. Dyson et al. and later Baker reported that bands of red blood cells were formed during exposure to ultrasound [54, 55]. Today, the phenomenon is utilized primarily for; air-levitators where small droplets or particles can be held in air without contact [56], separation of bioparticles in flowing liquid by acoustophoresis [57, 58], as well as the capture and retention of cells or microparticles in fluids through acoustic trapping.

From macroscale devices to lab-on-a-chip

Pioneering devices for acoustic trapping were developed by Coakley et al. [59] and later Hertz [60]. These and similar devices at the time were macro-scale devices utilizing large containers with multiple wavelengths across and often focused at increasing sedimentation rates for e.g. blood plasma production or to increase the rate at which functionalized particles interacted with each other by bringing particles together with acoustics instead of relying on random interactions to occur [61].

The concept of lab-on-a-chip or micro total analysis systems [6] (μTAS) was conceived in 1990. This led to a major shift in focus for large parts of the research community, and together with developments in microfluidics and micro-fabrication devices with complex networks of microfluidic channels was made possible. Thanks to laminar flow conditions in the microfluidic devices precise control of fluid movement was enabled. These developments subsequently were combined with acoustic trapping technology, which had a great influence on both devices and applications.

From affinity-assays to cell-studies

Early applications of acoustic trapping primarily concerned bead-based assays, such as agglutination or doublet assays [38, 62-64]. These rely on the formation of protein specific immuno-complexes and acoustic trapping provided a means to increase the likelihood of interactions between beads to occur. It was also shown that the sensitivity of singlet assays utilizing functionalized beads with fluorescent readout could be increased by collecting the beads in front of an optical sensor [65]. By doing this, the trade-off between optimal bead concentration for capture and optimal bead concentration for detection was eliminated.

Studies of cell viability in an acoustic trap [66-68] have opened up for the interesting prospect of making "in-trap cell assays". The viability of a variety of cells has been tested confirming that viability can be maintained in the acoustic trap. For yeast cells is has also been shown that cells can be cultured in the acoustic trap, if a continuous supply of nutrients and a controlled temperature is provided [36]. Obviously, the problem of cell viability too complex for one to make a general statement that all acoustic trap types are safe for all cell types. Studies of cell damage induced by exposure to ultrasound show that low frequencies and high intensities increase the risk of damage [69, 70]. Other studies have indicated that exposure to ultrasound is less damaging at high cell concentrations [71], and that exposure may increase the permeability of cells such that more effective transfection can be achieved [72, 73].

Layered resonators

The multilayer- or planar-resonator is a well-established method for designing an acoustic trap [74]. A vertical structure with wavelength matched layers is used to create an acoustic resonator. To create a particle-trap, lateral particle forces [75] are subsequently used to retain particles within the resonator. Three material layers are typically stacked on a piezoelectric transducer; a coupling layer for efficient transmission into the structure, a fluid layer where capture occurs, and a reflecting layer for retaining the acoustic energy in the device. By utilizing operation frequencies in the MHz-range and single or few trapping-nodes the fluidic layer can be scaled down sufficiently to allow laminar flow conditions, a design pioneered by Bazou et al. [76] as depicted in **Figure 6**a. With lateral dimensions much greater than the channel-height (high aspect ratio) the device can be modelled essentially as a 1D resonator, making optimizations simply a matter of optimizing the layer thicknesses [74]. The layered resonator design shown in **Figure 6**a has proven useful in optical cell-cell interaction studies[77-79]. In these studies, the acoustic forces were used to bring cells into close proximity to aid in optical-studies of the formation of gap-junctions and cytoskeletal reorganization.

In layered resonators the active region is typically defined by the size of the transducer. By having a localized actuation the ultrasonic standing wave can be laterally confined as to allow lateral particle forces. The layered resonator design can therefore be miniaturized by miniaturizing the ultrasonic transducer [80]. As shown in **Figure 6**b this technology enabled three trapping sites to be included in a microfluidic system for dynamic arraying [81].

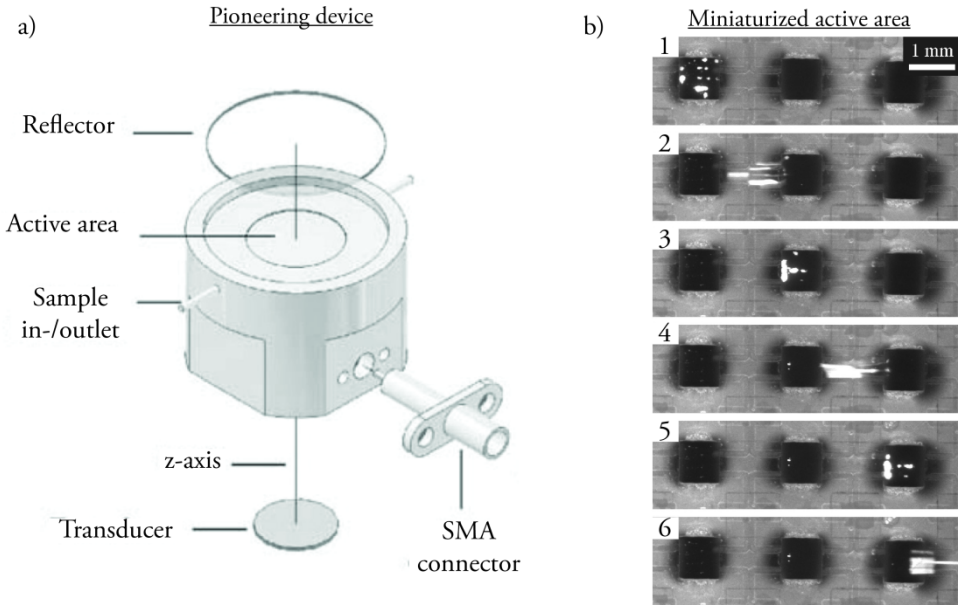

Figure 6: Comparison of a pioneering layered resonator device for acoustic trapping (a) and a variant utilizing three miniaturized transducers (b). In these device designs the trapping area is set by the size of the transducer, and in the case where three transducers are included in the channel dynamic control of the particle position can be obtained by turning transducers on and off with a flowing liquid (left to right).
Reprinted from Ultrasound Med. Biol., 31 (3), D. Bazou, et al., *Physical Enviroment of 2-D Animal Cell Aggregates Formed in a Short Pathlength Ultrasound Standing Wave Trap* , 423-430, Copyright (2005), with permission from Elsevier.
Reprinted from Sensor Actuat B-Chem, 106 (2), T. Lilliehorn, et al., *Dynamic Arraying of Microbeads for Bioassays in Microfluidic Channels*, 851-858, Copyright (2005), with permission from Elsevier.

Resonance cavities

In a microchip format, resonance cavities can be employed to localize acoustic energy and allow acoustic trapping. This is analogous to how cavity resonators can be constructed as waveguides for radio engineering [82, 83]. An early example of a cavity resonator was presented by Manneberg et al. [84], as depicted in **Figure 7**. A feature of this design is that the cavity can be actuated externally on the chip [85]. External actuation allows simultaneous use of multiple transducers for multiple-frequency actuation. This can be used to obtain 3D spatial positioning as well as an optically transparent device, both useful features for positioning in high-resolution optical characterization. A challenge with this design is retaining particles against high flow rates, as introducing a fluidic channel in the resonator constitutes a disturbance of the field. Recently, parallel cavity resonators actuated using a modulated frequency was used to realize parallel positioning of cells for optical study in a no-flow device [86]. This allowed parallel monitoring of several interaction events for natural killer cells where cells where brought into contact using acoustics [87].

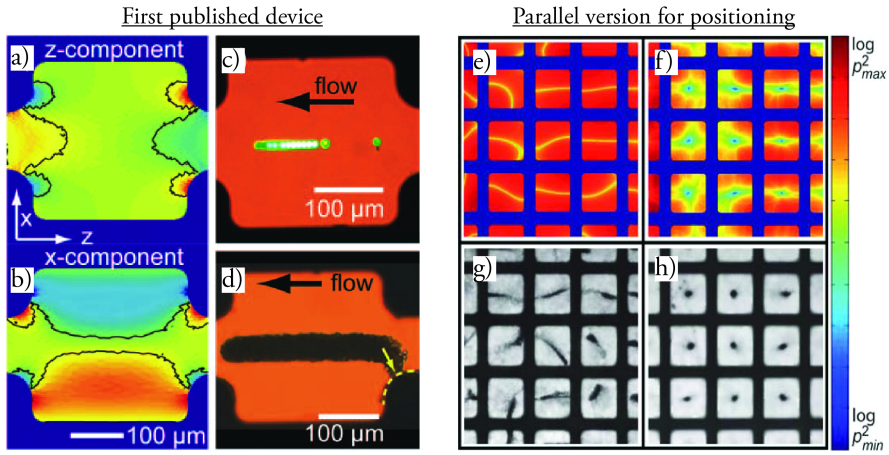

Figure 7: An early cavity resonator for acoustic trapping with simulations (a-b), and demonstration of particle capture (c-d). Recently frequency modulation has allowed this device concept to be parallelized. Here, simulations (e) and positions (g) for a single frequency shows large variations in position, whereas for a modulated frequency these differences can be averaged out showing predictable positioning in both simulations (f) and experiments (h).
Reprinted with permission from Appl. Phys. Lett., 93 (6), O. Manneberg, et al., *A Three-Dimensional Ultrasonic Cage for Characterization of Individual Cells*. Copyright 2008, AIP Publishing LLC.
Adapted from Lab Chip, 10 (20), B. Vanherberghen et al., *Ultrasound-Controlled Cell Aggregation in a Multi-Well Chip*, 2727-2732 (2010) with permission from The Royal Society of Chemistry.

Positioning and alternative devices

In contrast to applications where capture and retention is the primary objective, positioning of particles can in itself be an application. This can be accomplished using larger cavity resonators and harmonic resonances [88]. By tuning the actuation frequency a wide variety of interference patterns can be produced, and utilized for positioning. Recently many of the results for positioning obtained using bulk wave devices have been reproduced using Surface Acoustic Waves (SAW) [89]. This approach utilizes a surface wave that propagates along the interface between the liquid and a piezoelectric material (typically lithium-niobate) to create similar interference patterns. Although a piezoelectric substrate is needed, the lid of similar devices can be made of plastic – potentially making it slightly more low-cost than the bulk-wave counterpart. Perhaps more importantly, SAW devices might more easily facilitate extremely high-frequency devices as recently demonstrated by particle manipulation using a 133.3-MHz device [90]. Other alternative techniques to the microfabricatied resonance structures include trapping of particles in fluid by a focused acoustic beam [91] and the capture of particles close to a vibrating tip [92].

Trapping in capillaries

In the parts of my thesis focussed on device development, the possibility of combining glass capillaries with localized actuation for acoustic trapping is explored. Glass capillaries are an attractive option as they have good acoustic properties in terms of attenuation and speed of sound, and they are also inexpensive to mass fabricate and can be bought in a wide variety

of shapes and sizes. It has also been previously shown that capillaries can be used for acoustic trapping [37, 61]. The challenge for improvement has been to provide efficient actuation enabling a trap with good performance, as well as a low cost setup that match the low-cost and single-use potential of a capillary-based trap. As will be discussed in greater detail, the approach has been to utilize a rectangular cross-section capillary create a capillary trap that resembles a layered resonator with a miniaturized transducer.

2 Acoustofludics

The term acoustofluidics is a combination of the words acoustics and microfluidics and pertains to the physics applicable to microfluidic devices utilizing acoustics. The term was recently coined on a meeting in Udine, Italy 2011 that started[93] a 23-episode review series[64, 74, 94-112] on the subject. In these and other reviews[113], previous doctoral theses [114-117], and in textbooks on microfluidics [118, 119] and acoustics [120] both comprehensive and well-written texts on this subject are available. In light of this, the aim of this section is to highlight valuable insights on this subject and relate them specifically to acoustic trapping.

2.1 Microfluidics

Inertia is the tendency of something to remain unchanged. In physics, it is used to describe that matter has a property to remain in rest or in movement along a straight line unless perturbed by an external force. In the macroscopic world this property is very intuitive and often taken for granted. However, in a fluid on the microscale new intuition has to be developed.

Motion and other properties of a fluid are mathematically described using continuous fields, such as the vector field **v** that describes the velocity of the fluid at every point in the fluid. The Navier-Stokes equation is a general equation that describes the interaction of these fields,

$$\rho\left[\frac{\partial \mathbf{v}}{\partial t} + (\mathbf{v})\right] = -\nabla \mathbf{p} + \eta \nabla^2 \mathbf{v} + \mathbf{f}, \qquad \text{Equation 1.}$$

Here, **p** is the pressure scalar field, ρ is the density of the liquid, η is the viscosity and **f** is the forcing term. The forcing term is used to include bulk forces such as gravity or electrical forces in the model. This way of writing the Navier-Stokes equation emphasizes the analogy with Newton's second law by putting the inertial terms to the left and the force terms to the right. The two default force terms included in the model are the pressure gradient and the viscous drag.

2.1.1 Laminar flow

The Reynolds number quantifies the significance of inertia, and it is the quota between inertial and viscous parameters in the Navier-Stokes equation,

$$\mathrm{Re} = \frac{\rho L \mathbf{v}}{\eta}, \qquad \text{Equation 2.}$$

Here, L is a characteristic length scale of the system. The length scale basically works as a zoom for the physics and it can be selected as; the smallest dimension of a microchannel to study fluid flow in it, the diameter of a particle to study its immediate surroundings, or adjusted to some other feature of interest. At Reynolds numbers above 1500 turbulence becomes increasingly likely; at Reynolds numbers above one inertial-effects are still important; whereas at numbers below one they become increasingly negligible [116]. In microfluidic systems the Reynolds number is typically low, producing laminar flow conditions as demonstrated by the simulation (COMSOL Multiphysics, COMSOL AB, Sweden) in **Figure 8**. Under laminar flow the fluid flows in parallel layers without lateral mixing other than diffusion. This makes the flow in a microchannel easy to predict and allows reproducibility of flow conditions. For acoustic trapping this enables control of how much fluidic drag the trapped particles experience, control of particle delivery, and a way to control concentration and dose of different analytes.

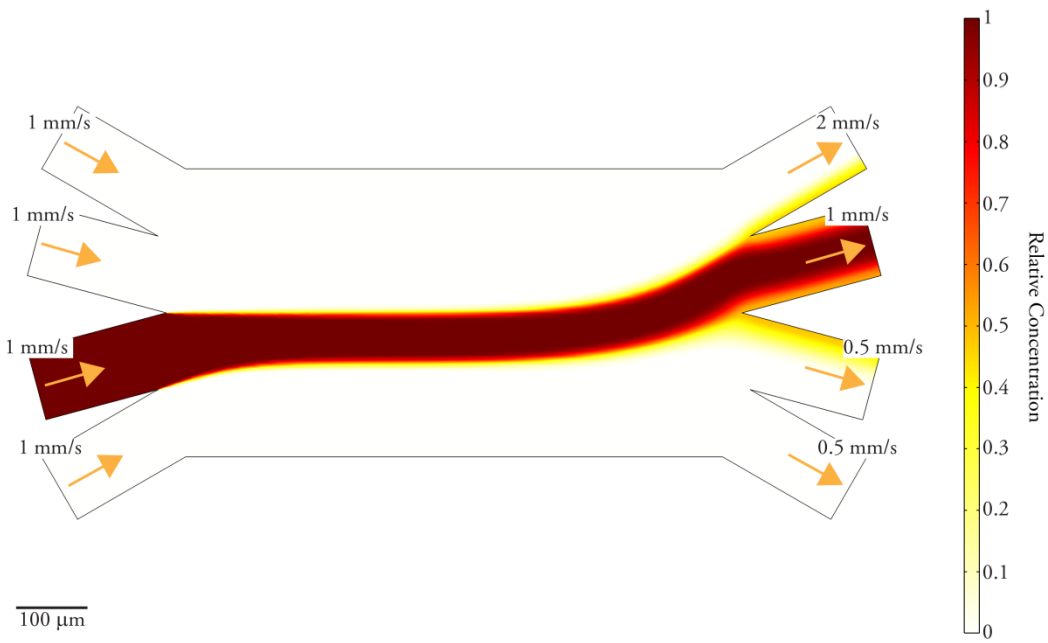

Figure 8: A simulation demonstrating flow in a microfluidic device. The colour gradient represents concentration of a chemical substance with a diffusion constant similar to that of a protein (D = 50 µm²/sec). The low Reynolds number (Re = 1.6) provides laminar flow conditions that allows the incoming stream to be directed to a specific outlet. The high Péclet number (Pe = 16 000) means only a minor portion of the infused substance will diffuse over to a parallel stream.

2.1.2 Parabolic flow profiles

Under laminar flow conditions, a pressure-driven flow in a microchannel will create a parabolic flow profile. This is due to the no-slip boundary conditions, stating that the velocity at the wall is zero. This condition is necessary for a continuous transition to a stationary solid-wall and the effects of this interface are transferred to the bulk liquid through viscosity creating the parabolic flow profile.

For a parallel plate geometry the Poiseuille flow profile provides an analytical solution for the velocity, v_x, along the pressure gradient,

$$v_x(z) = \frac{\Delta \mathbf{p}}{2\eta l}(h - z)z = \frac{6\langle v_x \rangle}{h^2}(h - z)z, \qquad \text{Equation 3.}$$

Here, $\Delta\mathbf{p}$ is the pressure difference along the channel, η is the viscosity of the liquid, z is the height position, and h is the distance between the parallel plates, **Figure 9**a. From an experimental point of view it is often more convenient to express the flow profile as a function of the average flow velocity $\langle v_x \rangle$ instead.

For a geometry which is significantly wider than it is high the parallel plate can be a good model. **Figure 9** shows a plot of the Poiseuille flow profile in comparison with a numerical simulation (COMSOL Multiphysics, COMSOL AB, Sweden) of the flow in a trapping capillary, which has a height of 200 µm and a width of 2 mm. As seen here the 1D model accurately describes the centre of the channel but needs adjustment close to the walls.

For particle capture, the parabolic flow implies that will arrive at a higher rate in centre of the channel, since the particle flux for a given segment scales with the flow velocity. For instance, the centre 50 % of the channel will have 68.7 % of the particles per second (pps), in a parallel plate approximation. In the acoustic trapping method described herein the trapping hotspot is typically in the centre of the channel, meaning that a higher fraction of particles will arrive close to it.

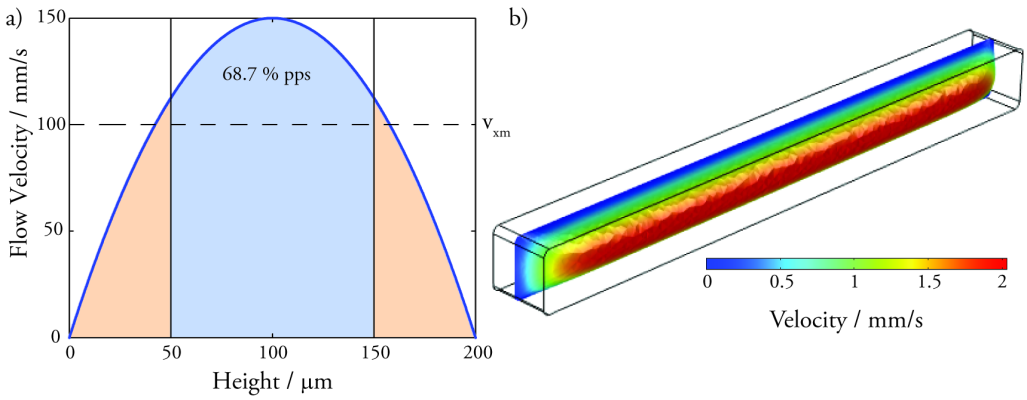

Figure 9: The parabolic flow profile between two plates with 200 µm spacing (a), and a simulation of the flow in a trapping capillary (b), which is 200 µm high and 2 mm wide. As seen, the plate approximation accurately describes the central parts of the channel but needs adjustment close to the wall.

2.1.3 Stokes drag

As a particle is moved in a liquid medium or as medium is moved over a particle a viscous drag will occur. The scaling of this drag is relevant to compare with the trapping forces that can be applied using acoustics. Under laminar flow conditions, the viscous drag F_d, on a spherical particle can be calculated using Stokes drag,

$$F_d = -6\pi\eta a v\,, \qquad \text{Equation 4.}$$

Expectedly, the drag is a function of fluid velocity v, and viscosity η. Interestingly, the drag is not a function of the cross-section area but only the radius a, of the particle meaning that the drag is only slowly decreasing with the size of the particle. The fact that the drag scales so slowly with size is not only an issue when trying to capture small particles but also interesting as it relates to the loss of inertial effects on the microscale.

2.1.3 Microscale diffusion

Advection is the process where matter, i.e. particles or a chemical species, is transported by fluid motion, as illustrated in **Figure 8**. The Péclet number describes the significance of advection in relation to diffusion,

$$\mathrm{Pe} = \frac{Lv}{D}\,, \qquad \text{Equation 5.}$$

Here, D is the diffusion constant for the particles or chemical substance. As mentioned earlier, L represents a characteristic length scale and v is the fluid velocity. In a microfluidic system with a low Reynolds number diffusion is solely responsible for mixing. Therefore the

Péclet number can be used to assess whether significant mixing will occur at the selected length scale.

For a particle, the diffusion constant can be calculated by the Stokes-Einstein relation,

$$D = \frac{k_B T}{6\pi\eta a}, \qquad \text{Equation 6.}$$

Here, k_B is Boltzmann's constant, T is the temperature, a is the particle radius and η is the viscosity of the media.

The seemingly straightforward calculation of diffusion constants quickly gets complicated when applied to biological samples. Here, a vast diversity of fluids and particles exist and oftentimes parameters such as viscosity and size have not been systematically characterized. One example is bacteria; the number of species in the human intestine [121-123] is estimated to about 400-500, or 500-1000 in the entire gut-microbiome [124, 125]. All these bacteria will have varying size and shape not only determined by species, but also depending strain, and individual variations caused by factors such as their phase in the reproduction cycle. Another example is the variety proteins, where the human genome encodes for 20 000-25 000 different kinds [126]. Thanks to mass spectrometric studies the mass in Daltons can typically be found for a specific protein. However, the radius depends on the folding of the protein and is not easily derived from the mass. Typically circumstances like these make calculations on the subject very approximate. One initiative to collect scientifically published data on physical parameters such as diffusion constants is the database BioNumbers [127].

The average diffused distance ⟨r⟩, for a particle displays an interesting time-dependence,

$$\left\langle \mathrm{r}^2 \right\rangle = 2k \cdot Dt, \qquad \text{Equation 7.}$$

Here, t is the time, and k is a dimensionality constant that is 3 for 3D diffusion in bulk, 2 for 2D diffusion e.g. in a lipid bilayer, or 1 for a 1D situation. Interestingly, the diffused distance is proportional to the square root of time making diffusion over short distances significantly faster than over longer distances. This time dependence is plotted in **Figure 10** showing the diffusion distance for a set of particles given in **Table 2.**

The diffusion of both small molecules and proteins can be important for an acoustic trapping application, as it determines what incubation times are needed when cells in a trapped cluster are exposed to a perfused substance. With the non-linear time dependence reducing the diffusion distances by for instance trapping particles in a thin layer may significantly shorten the incubation times when compared to a spherical cluster.

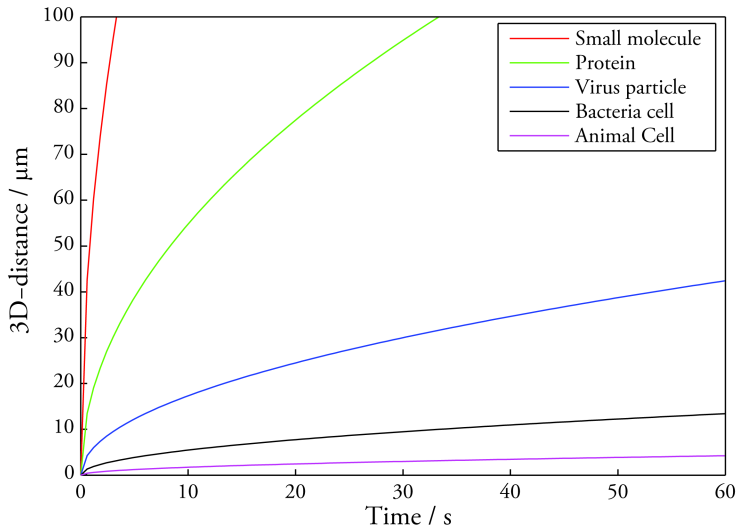

Figure 10: The diffusion distance as a function of time for different bioparticles, with diffusion coefficients as approximated in **Table 2**.

Table 2: Order of magnitude estimations of the diffusion coefficient for different bioparticles as given by Bray [128].

Particle	Small molecule	Protein	Virus particle	Bacterial cell	Animal cell
Diffusion coefficient / $\mu m^2/sec$	500	50	5	0.5	0.05

2.2 Acoustics

Fundamentally, acoustic waves are changes in the position of matter. This means that as an acoustic wave propagates through a medium, the position of the medium will be shifted with a distance that is determined by the wave-amplitude. The acoustic wave is described using a field that describes either the displacement itself ξ, the velocity of the displacement **v**, the scalar velocity potential ϕ, or the pressure changes **p**, associated with displacing the matter. Regardless of which aspect is used to describe the acoustic-wave it will obey the wave-equation that for velocity looks as follows (a forcing term **f** may also be included),

$$\frac{\partial^2 \mathbf{v}}{\partial^2 t} = c^2 \nabla \mathbf{v}\,, \qquad \text{Equation 8.}$$

Here, c is the speed of sound as it couples the change in position to the change in time. The speed of sound is a material parameter and can be found from the compressibility κ, and the density ρ, of the media,

$$c = \frac{1}{\sqrt{\kappa\rho}} = \sqrt{\frac{K}{\rho}}, \qquad \text{Equation 9.}$$

For some materials the bulk modulus K may be easier to find as it is more widely used in material sciences than is the compressibility. **Table 3** shows a list of parameters for materials utilized when building an acoustic trap based on glass capillaries.

Table 3: Shows a list of acoustically relevant parameters for materials used in an acoustic trap at 20 °C, the parameters of the physiological saline solution are calculated using a formula given in [129].

Material	Density / kg m^{-3}	Compressibility / 10^{-10} Pa^{-1}	Longitudinal speed of sound / m s^{-1}
Deionized water [130]	998.2	4.56	1482
Physiological saline solution (0.9 %) [129]	1005	4.48	1491
Pyrex glass [130]	2230	0.278	5674
Glycerol [130]	1261	2.19	1904

2.2.1 Resonance patterns

In a confined geometry with set boundary conditions the wave equation will have Eigen-modes and Eigen-values. The Eigen-mode corresponds to a pattern in the acoustic field that repeats itself over time, and the Eigen-value corresponds to the repetition frequency. With a repeating pattern in the acoustic field more and more energy can be added to the system if supplied with a matched frequency, thereby creating a resonating system.

At a given actuation, the resulting amplitude of a resonance field is determined by the amount of energy that can be stored in the mode and transferred to the system. This, in turn, is determined by the attenuation of the system and the coupling to the source of actuation. In an idealized system, simulations using finite element software allow easy calculation of the theoretically possible modes for specific geometry. However, including correct attenuation and realistic coupling to a source in the simulation is more challenging. Therefore, comparison with experimental data is useful to understand which of the theoretically possible modes will be relevant in practice.

In a macroscopic setting, direct measurement of the acoustic fields can be made using e.g. a hydrophone or a Schlieren system. In a closed microchannel no suitable system has yet been invented to measure these properties directly, however the acoustic field can be indirectly studied using the movement of microparticles. For microdevices, Hagsäter et. al. [131] pioneered this approach by comparing simulated fields to observed movement of both micron and submicron particles, **Figure 11**. Recently, this approach has been much refined through the use of micro particle tracking velocimetry in combination with mathematical models that can produce images of the acoustic field that are based on experimental data [132-134].

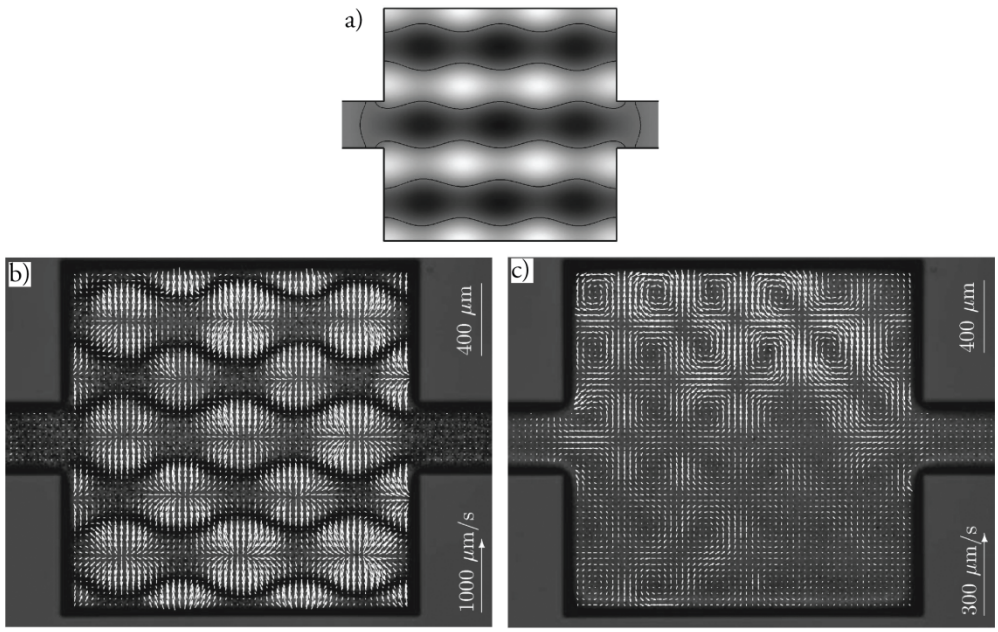

Figure 11: The simulation of the acoustic field in a resonance cavity (a) shows the pressure distribution for the used Eigen-mode. Nodal lines are shown in black and the grey colour-map shows local pressure at a fixed time. The primary acoustic radiation forces will push particles towards the nodal plane with a velocity set by the field gradients. The particle movements induced by the primary forces are shown by the arrows in b. For smaller particles acoustic streaming will dominate, the recirculating flows caused by acoustic streaming is shown by the arrows in c.
Adapted from Lab Chip, 7 (10), S. M. Hagsater, et al., *Acoustic Resonances in Microfluidic Chips: Full-Image Micro-PIV Experiments and Numerical Simulations*, 1336-1344 (2007) with permission of The Royal Society of Chemistry.

2.2.2 Primary radiation forces

The primary acoustic radiation force is the force exerted directly on a particle by an acoustic field. For a spherical particle with radius *a*, it is determined by the gradient (change) of both the pressure and the velocity field,

$$F_{rad} = -\frac{4\pi a^3}{3}\left[f_1 \frac{\kappa}{2}\nabla\langle p^2\rangle - f_2 \frac{3\rho}{4}\nabla\langle v^2\rangle \right], \qquad \text{Equation 10.}$$

The acoustic contrast factors f_1 and f_2 are respectively found by comparing the compressibility of the particle κ_p to that of the media κ, as well as the density of the particle ρ_p to that of the media ρ,

$$f_1 = 1 - \frac{\kappa_p}{\kappa}, \qquad \text{Equation 11,}$$

$$f_2 = \frac{2\left(\frac{\rho_p}{\rho} - 1\right)}{2\frac{\rho_p}{\rho} + 1}, \qquad \text{Equation 12.}$$

Interestingly, the f_1 factor is determined by compressibility difference and couples to the pressure gradient, and the f_2 factor is determined by density difference and is coupled to the velocity gradient.

In the simple case of a 1D standing wave, the relationship between the pressure and the velocity field is known allowing calculation of a single acoustic contrast factor (the Φ-factor). A thorough derivation of this is available in Mannebergs doctoral thesis [115]. The relationship between the fields in this case is prescribed by the boundary conditions and does not necessarily hold true for all circumstances. It can therefore be advantageous to use the f_1 and f_2 factors for a more generally applicable picture.

In non-contact acoustic trapping, three-dimensional forces are required to direct particles to a certain point in space. This means that velocity and pressure gradients are required in all three dimensions such that a potential minima is formed. Comparison of **Figure 11**a to **Figure 11**b shows how the gradient of the pressure field help direct particles to the nodal positions and how the particles move with a greater velocity where there is a sharp pressure gradient. In a cavity resonator such as this, these forces will be useful for trapping in the sense that they will position particles in the lateral plane. To achieve non-contact trapping a vertical resonance would also be required to lift and position particles vertically.

Calculation of the acoustic contrast factors requires the density and compressibility of specific bioparticles. Thanks to a variety of measurement methods and the widespread use of for instance gradient centrifugation it is not uncommon to find the density of different bioparticles in the literature. However, up until recently the compressibility (bulk modulus) has only been thoroughly investigated for red blood cells [135], as they are important when doing ultrasonic imaging. In 2011 both Barnkob et al. [136] and Hartono et al. [137] reported values for the compressibility of different cells. The results from these characterisations are given in **Table 4**, together with references to the respective original publications. Slightly different approaches to determining the compressibility were used: Barnkob et al. used a 2D image of the field and determined both density and compressibility from the cell movement in this field, whereas Hartono et al. used a 1D standing wave approximation of the field and literature values for the density. The simultaneous measurement of density may here be advantageous as the density can be determined for the individual cell, in contrast approximating a constant density which will transfer errors in density to the estimation of compressibility. However, one may anticipate that the estimation of cell size will infer the largest error as the particle velocity scales with the square of the radius (compare Equation 4 and Equation 10). In spite of these limitations, these reports provide reasonable approximations three normal cell samples and four cancer cell lines. While an almost infinite amount of bioparticles still remains to be characterized, these publications constitutes an important step forward to enable better estimations to be adopted these cell types and similar bioparticles.

Table 4: Reported values on compressibility and density for different cells, in relation to that of polystyrene particles.

Particle	Density / kg m^{-3}	Compressibility / 10^{-10} Pa^{-1}
Polystyrene bead	1050	2.16 ± 0.18
Red blood cell [135]	1099	3.31 ± 0.22
White Blood cell [136]	1019 ± 1	3.995 ± 0.012
Prostate cancer cell line (DU145) [136]	1018 ± 1	4.239 ± 0.006
Breast cancer cell line (MCF-7) [137]	1068	4.22 ± 0.19
Liver cancer cell line (HEPG2) [137]	1087	4.28 ± 0.12
Colon cancer cell line (HT-29) [137]	1077	4.04 ± 0.16
Fibroblast (NIH/3T3) [137]	1079	3.78 ± 0.17
Breast cell (MCF-12A) [137]	-	3.77 ± 0.09

2.2.3 Secondary radiation forces

Secondary radiation forces or inter-particle forces are a result of acoustic waves being scattered from one particle to another. If the incident field is a plane wave the secondary radiation force between two identical particles can be derived as [75],

$$F_{Sec} = 4\pi a^6 \left\{ \frac{\left(\rho_p - \rho\right)^2 \left(3\cos^2\theta - 1\right)}{6\rho d^4} v^2(x) - \frac{\omega^2 \rho \left(\kappa_p - \kappa\right)^2}{9d^2} p^2(x) \right\}, \qquad \text{Equation 13.}$$

Here, ω is the angular frequency, d is the inter-particle distance (centre-centre), and θ is the angle between the axis of the incident wave and the centreline connecting the two particles. The force is defined such that a negative force should be interpreted as an attractive force between the particles. A schematic drawing of how the angle and distance is defined with respect to the incident wave is found in the first figure in Paper II.

Note that the secondary radiation force scales heavily with the distance between the particles. As the magnitude drops of so rapidly with particle spacing the effects of the secondary radiation force can be ignored in many cases. When acoustically trapping particles in a tight cluster there is, however, reason to believe that these effects are significant.

The equation for secondary radiation force is derived under the assumption that the incident field is a plane wave. This is of course a limitation when applied to the complex fields utilized for acoustic trapping. On the other hand, one may be reminded that as the force is only significant at very short distances where a plane wave approximation may perhaps be less offensive.

Interestingly, the secondary radiation force has two terms; one that is always attractive, and one that is angle-dependent. As the angle dependent term diminishes faster with the distance between the particles there will be an equilibrium-distance to witch a particle is

drawn [138]. The equilibrium distance will be angle dependent, such that at some angles the particles will tend to be as close as possible, whereas at other angles a small separation will be preferential. As both fluidic drag and primary radiation forces are typically active simultaneously with the secondary forces one has to consider these as well when trying to determine the final positions of the particles.

While the formula for the force is given for two identical particles in reality there will of course be secondary forces between particles with different sizes and properties. When attempting capture of nanoparticles it can, as will be shown later, be useful to utilize a larger particle to exaggerate the effects on a smaller particle.

2.2.4 Acoustic streaming

The acoustic fields will not only create forces on particles in the media, it will also create forces on the media itself. This phenomenon is known as acoustic streaming, and what is typically observed are rotational flows called streaming rolls. Classically three kinds of streaming at different length scales have been described. Here, Eckart streaming has container scale streaming rolls [139], Rayleigh streaming concerns wavelength scale rolls [140], and Schlichting streaming implies submicron flows within the viscous boundary layer of a wall [141].

The classically discussed streaming types all concern streaming perpendicular to the transducer (i.e. along the axis of the acoustic wave). In the device used in this thesis and in other layered resonators [142, 143] a prominent feature is streaming in the transducer plane (Paper II). This occurs as four streaming rolls above the transducer, and was recently modelled theoretically by Lei et al. [144], showing impressive correlation with the experimentally observed behaviour, **Figure 12**.

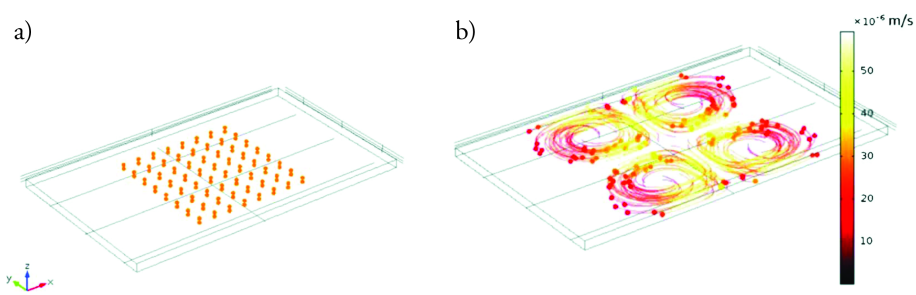

Figure 12: A simulation of the lateral streaming rolls that occur parallel to the transducer in the case of a localized resonance. The images show how an initial distribution of tracer particles (a) is affected by the induced streaming (b).
Adapted from Lab Chip, 13 (11), J. J. Lei, et al., *Acoustic streaming in the transducer plane in ultrasonic particle manipulation devices*, 2133-2143 (2013) with permission from The Royal Society of Chemistry.

In acoustic trapping the streaming is very important as it creates a fluidic drag on the particles. The fluidic drag creates a limit for the smallest particle size that can be trapped [145]. This concept is demonstrated clearly in **Figure 11** where **Figure 11**c shows the acoustic

streaming of submicron particles, **Figure 11**b shows larger particles dominated by the radiation forces, and **Figure 11**a shows the field responsible for these effects. The large scale lateral streaming rolls described in **Figure 12** also has implications for delivery of particles to the trapping site and in influencing mixing/incubation-times for in-trap assays.

2.3 Piezoelectric transducers

A piezoelectric transducer (piezo) consists of a piezoelectric material with at least two electrodes where an electrical signal can be applied or measured. The piezoelectric material has such properties that applied mechanical stress will generate an electric displacement. This creates a gradient in the electric potential along the direction of the applied stress, allowing a voltage to be measured over the material. The converse piezoelectricity is the reverse of this process, allowing an electrical field to generate a mechanical strain, **Figure 13**. The converse piezoelectricity is what is used to drive the acoustic resonator to create an oscillating system. The piezoelectric effect, as will be demonstrated later, can be utilized to analyse changes in the acoustic oscillator.

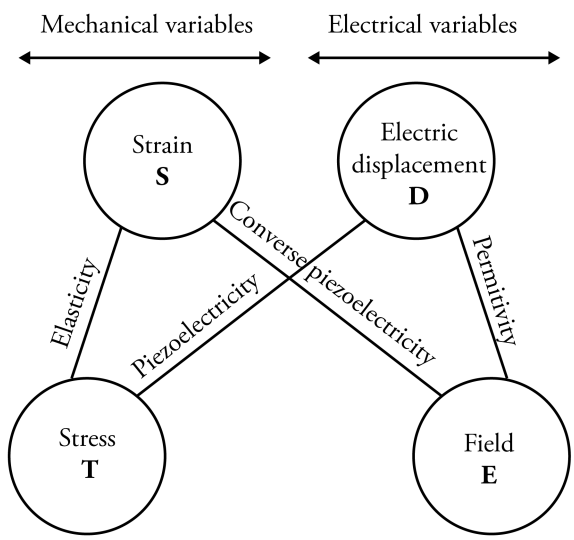

Figure 13: The piezoelectric effect and the converse piezoelectric effect allow conversion between electrical and mechanical energy.
Reproduced with permission from A. Janshoff, et al, *Piezoelectric Mass-Sensing Devices as Biosensors - An Alternative to Optical Biosensors?*, Angew Chem Int Edit (2000) 39 (22), 4004-4032. Copyright Wiley-VCH Verlag GmbH & Co. KGaA.

2.3.1 Piezoelectric material

One of the most common piezoelectric materials for creating an acoustic transducer is lead zirconate titanate (PZT). PZT is a ceramic material and exist in a variety of different grades that are specialized for different applications. In applications requiring continuous operation and low losses a hard grade such as PZT-4, also known as pz-26 or Navy-I, is suitable. **Table 5** shows the frequency constant and the coupling factor for this grade. These are two important parameters when designing a transducer for efficient trapping, and are provided in the datasheet [146]. The frequency constant is half the speed of sound and defined as the product of the fundamental resonance and the length. The electromechanical coupling factor is the efficiency of the conversion between mechanical and electrical energy, with a value of one meaning perfect coupling. As can be seen in **Table 5** both the speed of sound and the efficiency depends on the vibrational mode in the crystal. The vibrational mode is determined not only by the direction at which the sound travels but also by the dimensions of the piezo. As the piezo can be cut into any shape, the resonances in a non-standard geometry are typically determined experimentally by impedance analysis.

Table 5: Given frequency constants and coupling factors for PZT-4 at different vibrational modes [146].

Vibrational mode	Frequency constant / Hzm	Coupling factor
Radial mode	$N_p = 2230$	$k_p = 0.57$
Thickness mode	$N_t = 2040$	$k_t = 0.47$
Traverse length mode	$N_{31} = 1500$	$k_{31} = 0.33$
Longitudinal length mode	$N_{33} = 1800$	$k_{33} = 0.68$

2.3.1 Electrical model of a piezoelectric transducer

A piezoelectric transducer can be modelled using a piezoelectric resonator circuit, **Figure 14**. The mechanical properties of the transducer are represented by R_m, L_m and C_m. Qualitatively, the resistance, R_m, can be interpreted as a measure of the amount of losses in the crystal. This means that adding a load to the piezo by for instance changing the surrounding media from air to oil would increase the resistance. Similarly, the inductance, L_m, and the capacitance, C_m, are representatives of the kinetic and potential energy in the oscillator. The capacitance C_0, on the other hand, is simply determined by the electrical capacitance between the electrodes, and does not have a mechanical analogue.

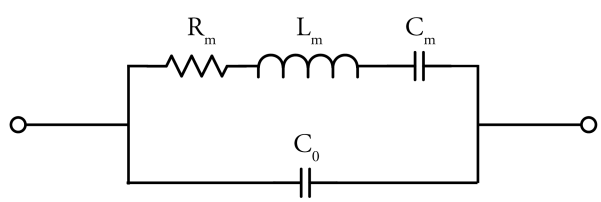

Figure 14: An equivalent circuit of a crystal resonator that can be used to model the ultrasonic transducer.

In order to evaluate the electrical model, the measured impedance can be compared to the impedance of the crystal oscillator circuit model. The impedance, Z, of such a system can either be derived using basic circuit theory, or found and explained in the literature [147, 148],

$$Z = \frac{\omega^2 L_m C_m - 1 - j\omega C_m R_m}{\omega^2 C_0 C_m R_m + j\omega^3 C_0 L_m C_m - \omega(C_0 - C_m)}, \qquad \text{Equation 14.}$$

To simplify the calculations needed for further analysis it is more practical to look at the admittance *Y*, of the resonator,

$$Y = \frac{1}{R_m + j\omega L_m + \frac{1}{j\omega C_m}} + j\omega C_0, \qquad \text{Equation 15.}$$

Here, the mechanical properties and the electrode capacitance are separated into two terms making the analysis easier. Both impedance and admittance are complex numbers, and it is therefore helpful for visualization and analysis to separate the frequency response into two variables. This can be done using either polar coordinates giving absolute admittance $|Y|$, and phase θ, or, into real and imaginary parts giving conductance G, and susceptance B,

$$G = \mathrm{Re}\{Y\} = |Y|\cos\theta = \frac{R_m}{R_m^2 + \left(\omega L_m - \frac{1}{\omega C_m}\right)^2}, \qquad \text{Equation 16,}$$

$$B = \mathrm{Im}\{Y\} = |Y|\sin\theta = \frac{\omega L_m - \frac{1}{\omega C_m}}{R_m^2 + \left(\omega L_m - \frac{1}{\omega C_m}\right)^2} + \omega C_0, \qquad \text{Equation 17.}$$

Interestingly, the conductance is independent of the capacitance C_0, leaving only mechanically related parameters in the equation. This makes the conductance highly suitable for evaluating the mechanical properties of the transducer. The conductance is essentially described by the so called *universal resonance curve* [83]. This equation is found in many physical circumstances where resonance is involved. Here, the mechanical resonance, ω_0, of the piezo is given by the frequency that has the maximum conductance, resulting in,

$$\omega_0 = \frac{1}{\sqrt{L_m C_m}}, \qquad \text{Equation 18.}$$

The mechanical quality factor or Q-value describes the quota between how much energy is stored in the oscillator and how much energy that is dissipated during one cycle. This is essentially the width of the resonance curve in relation to its height, and describes how efficient the system is. From standard analysis of the universal resonance curve it follows that at resonance it can be found using,

$$Q_m = \frac{\sqrt{L_m}}{R_m\sqrt{C_m}}, \qquad \text{Equation 19.}$$

To provide some intuition on the electrical parameters relate to the mechanical properties of a transducer **Figure 15** is included. Here, three different cases are shown with electrical parameters given in Table 6. Case 1 shows the curves obtained for reasonable parameters [149] describing a mounted PZT transducer used in acoustic trapping. Here, the peak and width of the conductance curve shows the mechanical resonance and Q-value. In the impedance curve the electrical series and parallel resonances can also be seen. The series resonance is the point of minimal impedance and is very close to the mechanical resonance in frequency. The parallel resonance is far from the mechanical resonance and is the point of maximum impedance. In the literature the parallel resonance is also commonly referred to as the anti-resonance.

Case 2 shows the effect of increasing the mechanical Q-value one order of magnitude while leaving load, R_m, unchanged. As expected the width of the conductance curve is much narrower, and also the distance between series and parallel resonance is smaller. Case 3 shows how an increased load at an unchanged mechanical Q-value would look. Here, height of the conductance curve is increased but the relative width is the same, and the distance between series and parallel resonance is increased. Relating back to the electrical properties of an acoustic trap, one may expect that the mechanically related circuit components will be affected by the mounted capillary and the acoustic properties of its content.

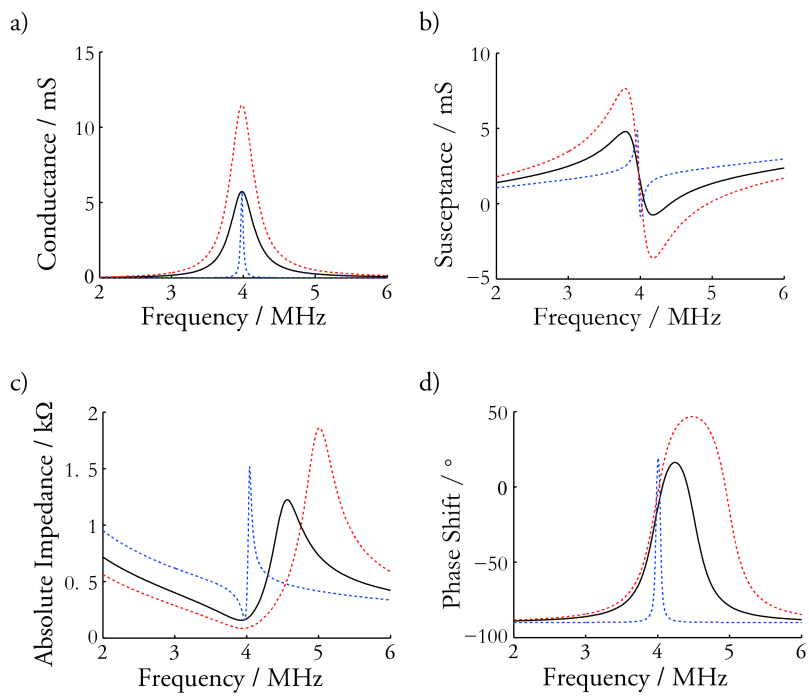

Figure 15: Impedance and admittance characteristics for an idealized crystal resonator. Three cases are represented with the circuit parameters given in **Table 6**.

Table 6: Case 1 represents reasonable model values for a mounted PZT transducer used in acoustic trapping at 4-MHz. To illustrate how changes in the transducer properties would affect the electrical characteristics case 2 and case 3 are included.

	f_0 / MHz	Q_m	R_m / Ω	L_m / μH	C_m / pF	C_0 / pF
Case 1	3.98	10	174.40	438	144.1	506.03
Case 2	3.98	100	174.40	4380	14.41	506.03
Case 3	3.98	10	87.20	219	288.15	506.03

3 Technology developments

In this section this section I will focus on the efforts to develop the technology platform for acoustic trapping. This includes: some fundamentals on how to utilize resonance in a glass capillary to achieve trapping, how to achieve an efficient actuation that allows automatic frequency tracking, capture mechanics that allow nanoparticle capture, and practical integration with bench top laboratory instruments such as MALDI-MS.

3.1 Acoustic trapping in a glass capillary

Acoustic forces on particles will occur where gradients or changes in local pressure and velocity amplitude exist. From this follows that changes in the acoustic intensity will infer forces on particles. To create a situation where the acoustic forces provide an opportunity for trapping particles, a spatial control or localization of the acoustic energy is needed.

One of the more straightforward ways to generate a suitable acoustic gradient for particle capture is to utilize localized actuation of a glass capillary, **Figure 16**. The idea is that the sound intensity will be significantly higher close to the point of actuation (i.e. the transducer) than elsewhere. As shown in Paper I, the principle of localized actuation can be used to generate an acoustic gradient that produce force on particles counteracting fluid flow in the channel. Herein, trapping was achieved in rectangular cross-section capillaries with millimetre-sized actuation sites.

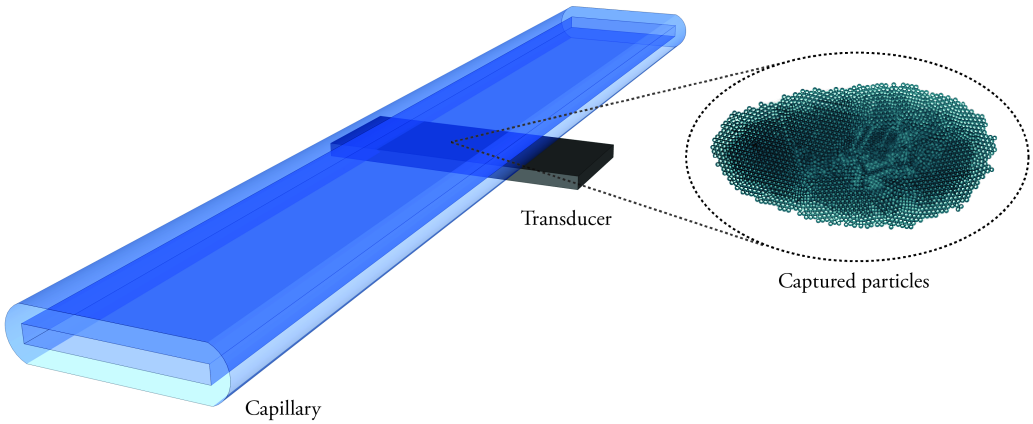

Figure 16: A schematic showing the essential parts of the device, consisting of a rectangular cross-section capillary and a transducer. Here, a cross-sectional resonance is locally actuated and the extent of the transducer defines the width of the trapping site, while the resonant mode pushes the particles to the centre of the channel to form a close-packed layer.

The most important aspect to provide optimal conditions for trapping is to utilize an acoustic resonance in the capillary. This greatly amplifies the sound intensity in the channel, turning the acoustic forces from a marginal effect into something that is practically useful. The geometry of the used capillaries dictates that the cross-sectional resonances are most important in the 1-15 MHz frequency range.

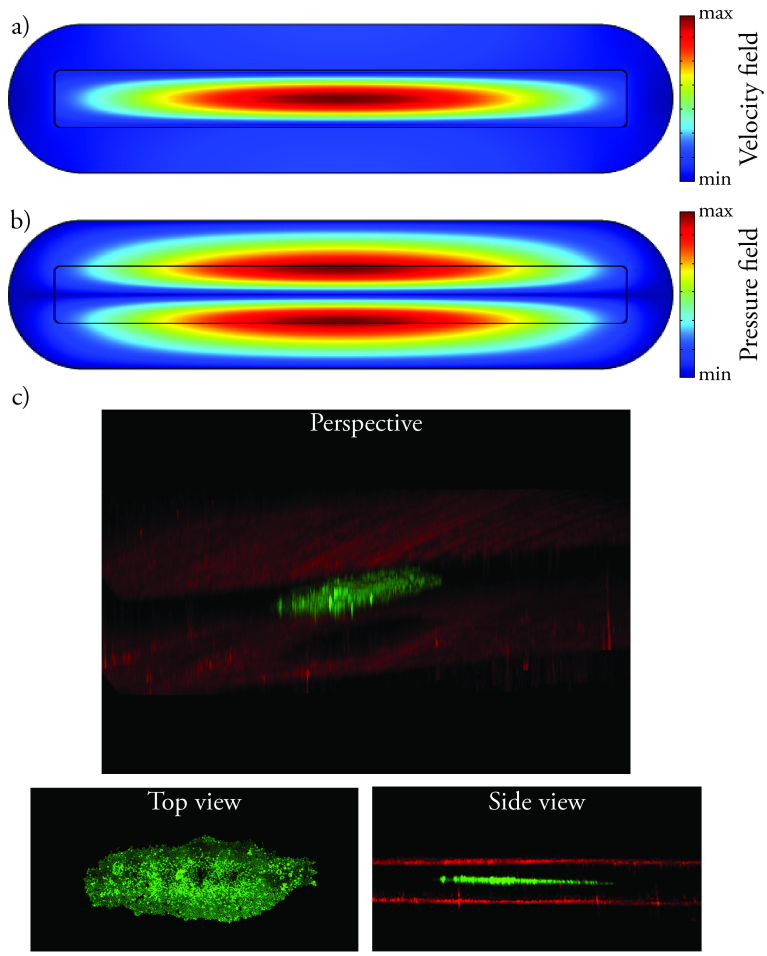

Figure 17: By comparing the simulated acoustic fields (a-b) to confocal data of the distribution of captured beads (c) one can obtain a good perception of how the thin layer of captured particles is positioned in the channel. The particle movement created by the simulated fields the particles is directed towards the positions with maximal velocity and minimal pressure. The confocal data shows the conformation of captured green fluorescent 4.2 µm particles and red reflections from the channel walls.

Utilizing cross-sectional resonance modes does not only increase the acoustic energy in the channel but it also allows some control of the cluster conformation. **Figure 17** shows the 4-MHz cross-sectional mode that is suitable for acoustic trapping in a 200×2000 μm^2 capillary, as well as confocal micrographs of the distribution of trapped particles using this mode. As seen here the resonance mode allows non-contact trapping of the particles as they are not only forced to stay above the transducer but also pushed to the centre of the channel in a thin layer.

Displayed here is the fundamental resonance mode that corresponds to the channel thickness, however there are many harmonics and combination modes available for excitation. For instance, it is shown in Paper I how three particle layers can be generated by

tripling the excitation frequency. It is in fact possible to combine fundamental resonances and harmonics from different dimensions to form 3D resonances producing a variety of patterns. While such modes can be observed in this device under stop flow conditions, they have generally been too weak to be suitable for trapping. An interesting use of such resonances is mode hopping [150] that can be observed by varying the actuation frequency under stop flow conditions. **Figure 18** shows an example of this where particles are moved to different positions based on the selected frequency, which can be both entertaining and potentially useful [151].

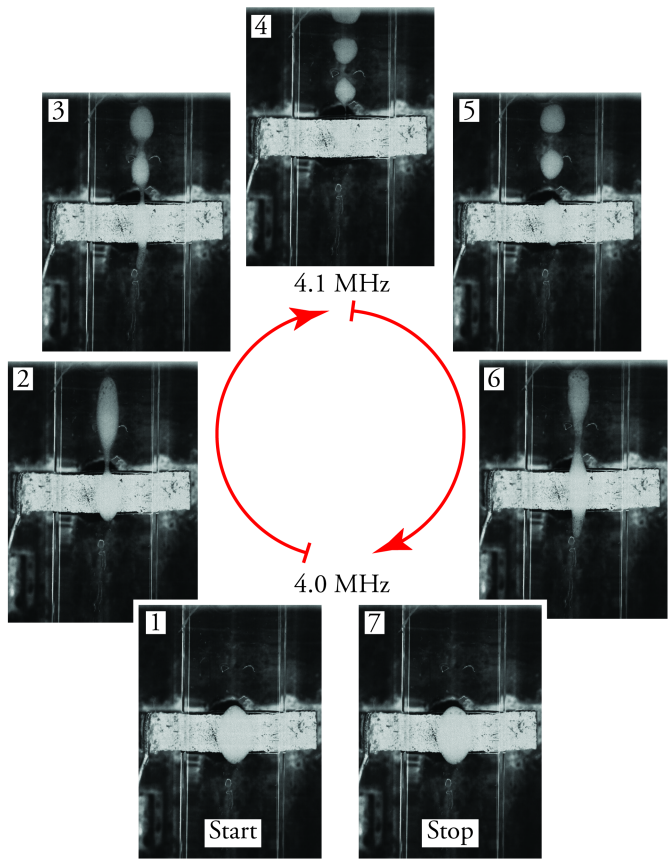

Figure 18: By sweeping the frequency under stop-flow conditions several weaker acoustic modes can be observed. As these modes are created by high overtones in the system they are very sensitive to changes in for instance the mounting, position of the transducer, and sample properties. In this particular case, several small clusters are created in front of the transducer (towards the open end) as the frequency is increased. Interestingly, the same modes reoccur when the frequency is decreased showing that the modes are specific states of the system.

The acoustic trapping here was done in rectangular cross-section capillaries. The reasons for choosing this geometry above the more easily fabricated circular cross-section are twofold; coupling to a flat surface mounted transducer is more practical, and the acoustic forces scale with the frequency of the ultrasound. For the force scaling, high aspect ratio geometries

allow a high frequency while having a larger channel that reduces the fluidic drag. This is important for throughput as it allows a higher volumetric flow rate to be used, by effectively parallelizing several smaller circular cross-section capillaries.

One aspect of the design that may be easily overlooked is the fact that the walls of the glass capillary have sub-wavelength thickness. Intuitively one might anticipate this to be an important feature in localizing the sound to the transducer site. Although experimental verification is lacking, due to the limited commercial availability of capillaries with different dimensions, one can compare with devices used for acoustophoretic separations described in the literature [58]. These devices can be a glass-silicon [152] or glass-glass chip [153] that has plenty of material surrounding the liquid channel. In this situation trapping does not generally occur and acoustic forces are distributed over the entire channel. It is important to note the limitations of such a comparison since the means of actuating the separation chips differs for how the capillaries are actuated.

3.2 Device improvements

3.2.1 Chip design, manifolds and fluidics

During the work with this thesis a variety of transducer mounting protocols and manifolds for assembling the capillary and the transducer have been used. While this may seem more of an engineering problem than a scientific problem, it is important to remember that the acoustic waves are mechanical vibrations and that the entire assembly will be part of the resonator. The guidelines in the evolution of new devices have been to minimize attenuation for a high mechanical Q-value, and to make the device as reproducible, simple and low-cost as possible.

To provide electrical connection to the small piezoelectric element some kind of packaging is needed. A standard in the electronics industry is to use printed circuit boards (PCBs) to mount electrical components. Surface mounting the piezo on a PCB using low-temperature solder and an oven provides an easy and scalable way of connecting to one side of the piezo. By drilling a hole in the PCB before mounting an air-backing can also be included. The advantage with including an air-backing is that the large difference in acoustic impedance between air and piezo reflects the sound back into the device maintaining a high Q-value on the transducer.

It is more challenging to connect to the surface facing the capillary. In Paper I where 1×1 mm^2 piezoelectric elements were used a complex protocol had to be adopted. First the piezo was cast in epoxy which had to be polished down to reach the surface of the piezo. This was a problem as over-polishing introduced a lot of variations between devices and the process was manual and tedious. After polishing, a thin metallic layer was evaporated onto the piezo and epoxy providing the necessary contact. This also introduced some problems as scratches and wear on the metallic layer drastically reduced the lifetime of the devices. In the end, devices such as shown in **Figure 19**a were produced where the capillary could be pressed

down onto a flat surface containing the transducers. In later designs it proved possible to use a transducer that was wider than the capillary, **Figure 19**c. This can be understood as the used cross-sectional resonance pattern (**Figure 17**a-b) inherently confines the trapping site in the lateral direction of the capillary. This allows the top-contact to be accomplished by simply soldering a thin wire from the top of the piezo to the PCB substrate. Again, this allows the entire transducer chip to be oven-soldered in a single step leading to increased reproducibility. As this mounting procedure doesn't produce a flat surface in level with the transducer to which the capillary can be pressed, a more advanced manifold is required. By using a precision milling machine a socket for the transducer chip can be made, such that the capillary touches only the piezo and two supports far away from the trapping site.

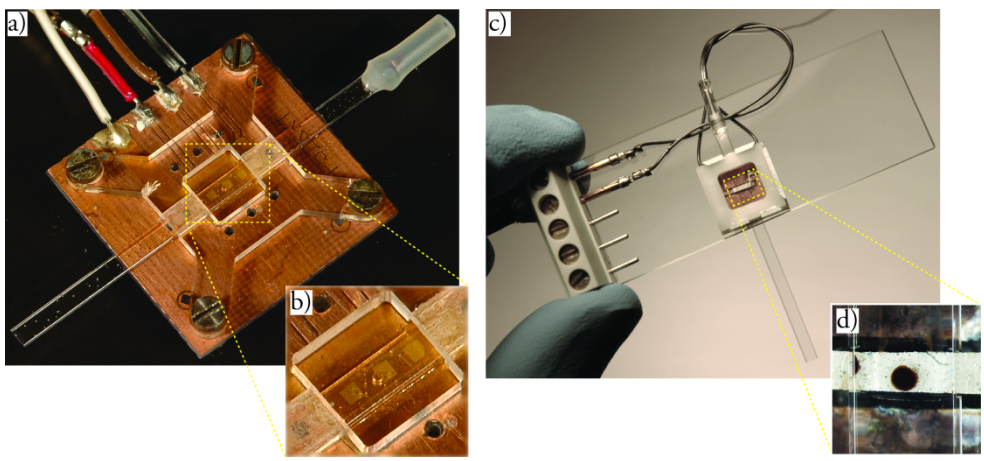

Figure 19: A comparison two manifolds used for assembly of transducer and capillary. In the early devices (a) the transducer elements are cast in an epoxy layer providing a flat surface towards which the capillary is pressed. Here, three 1×1 mm^2 transducers are distributed along the capillary providing three separate trapping sites (b). In the later version of the device (c), a precision milled holder allows the capillary to be pressed towards the transducer without having a flat surface. The close-up of the trapping site (d) shows that the transducer can be made wider than the capillary and still function – greatly simplifying the device fabrication.

There are several ways to provide a fluidic interface to the capillary. For the most part, a simple rubber tube glued to one end of the capillary will do the trick. There are however situations where one would like to interface the capillary with a more complex microfluidic system, e.g. to provide hydrodynamic pre-focussing of particles. In **Figure 20** two such approaches are demonstrated. The first one shows the capillary being included in a polymethylmetakrylate (PMMA) chip with microfluidic channels. This was accomplished by adjusting the channel dimensions to the external dimensions of the capillary and gluing it into place. The other example is based on inserting smaller capillaries into the trapping capillary and again sealing with glue. Recently Evander et al. reported a reversible seal between capillary and chip based on a polydimethylsiloxane (PDMS) gasket [154].

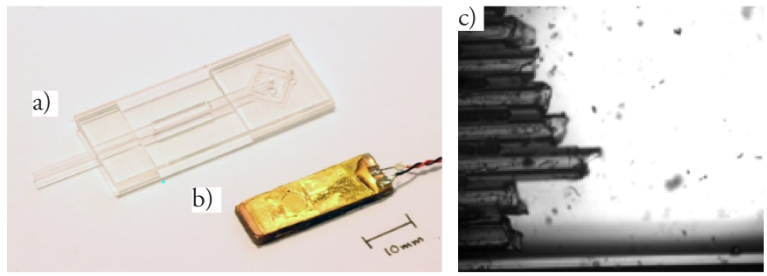

Figure 20: Two alternative methods for providing a multi-channel interface to the capillary. The capillary can be included in a plastic chip with microfluidic channels, such as the two-inlet PMMA device (a-b), or several smaller capillaries can be inserted into the larger capillary (c), in this case providing twelve separate inlets.

3.2.2 Kerfed transducers

In principle, the performance of the acoustic trap can be enhanced by increasing the power that the system is actuated with. In practice, increased temperature caused by the losses in the system is typically the limiting factor. In functional cell studies this limitation can set in early as the temperature should typically be kept no higher than 37°C. Even with a feedback controlled temperature regulator this can be challenging if too much heating is generated locally by the transducer. The gains from an increased acoustic output can however be profound since the primary acoustic radiation forces scale with the power of two to the amplitude of the acoustic wave[155]. Therefore the power conversion efficiency of the transducer is a key aspect in enabling a high-performance acoustic trap. To achieve an efficient resonator it is desired to have a sufficiently high piezoelectric coupling coefficient, a high Q-value, and a resonator free of spurious modes [156, 157].

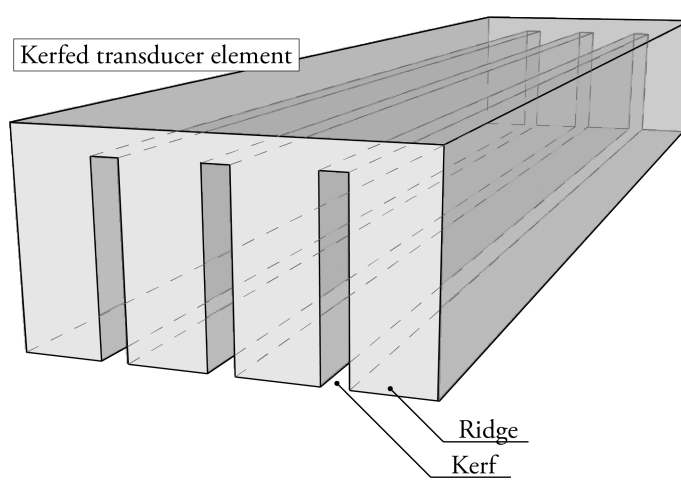

Figure 21: The resonance frequencies of vibrational modes in the transducer are determined by its dimensions. In the kerfed transducer, thin ridges are formed by partially cutting through the transducer. This process gives the lateral modes a high resonance frequency and prevents them from interfering with the used thickness-mode.

When utilizing a miniaturized transducer the interference from spurious modes can be significant[80]. In Paper IV a new way of designing miniaturized transducers that alleviates these problems is proposed and demonstrated. Here, removal of spurious modes in it is done by kerfing, i.e. partially cutting through the transducer, **Figure 21**. This method has long been used for controlling spurious resonances and creating individually accessible elements in advance transducers for ultrasonic imaging [158]. Spurious resonances arise when two transducer dimensions are to close such that their resonances are both present within the desired bandwidth. For a miniaturized transducer operating in the 4-MHz range this is a real issue, as the thickness of the transducer is approximately half a millimetre while the lateral dimensions are also on the millimetre scale. This creates interfering lateral modes in the piezo. Spurious modes can either be moved up in frequency by cutting the transducer or moved down in frequency by making the transducer longer. Moving the spurious modes to higher frequencies is typically the ideal method, as downward-shifted resonances will still interfere to some extent by their harmonics. For sufficient removal by upward-shifting a width to height quota of 0.6 has been suggested [159].

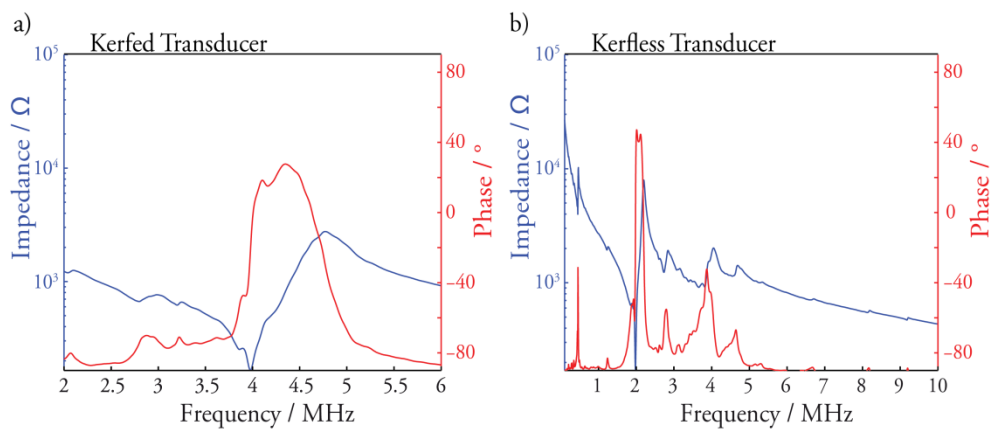

Figure 22: Comparing the impedance spectrums from the finished kerfed and the kerfless transducers shows how kerfing can be used to remove interference from lateral modes, producing a transducer that is dominated by the thickness mode. Note that the plotted frequency range has been made wider in b to clearly show the 2-MHz lateral resonance.

Figure 22 shows an impedance comparison between a kerfed and an un-kerfed transducer when mounted on a printed circuit board. The comparison shows efficient removal of the spurious resonances through kerfing. Some harmonic interference is still visible in the kerfed transducer from the length of the ridges. However, one can clearly see that these interferences are not as significant as the ones previously caused by the lateral resonances.

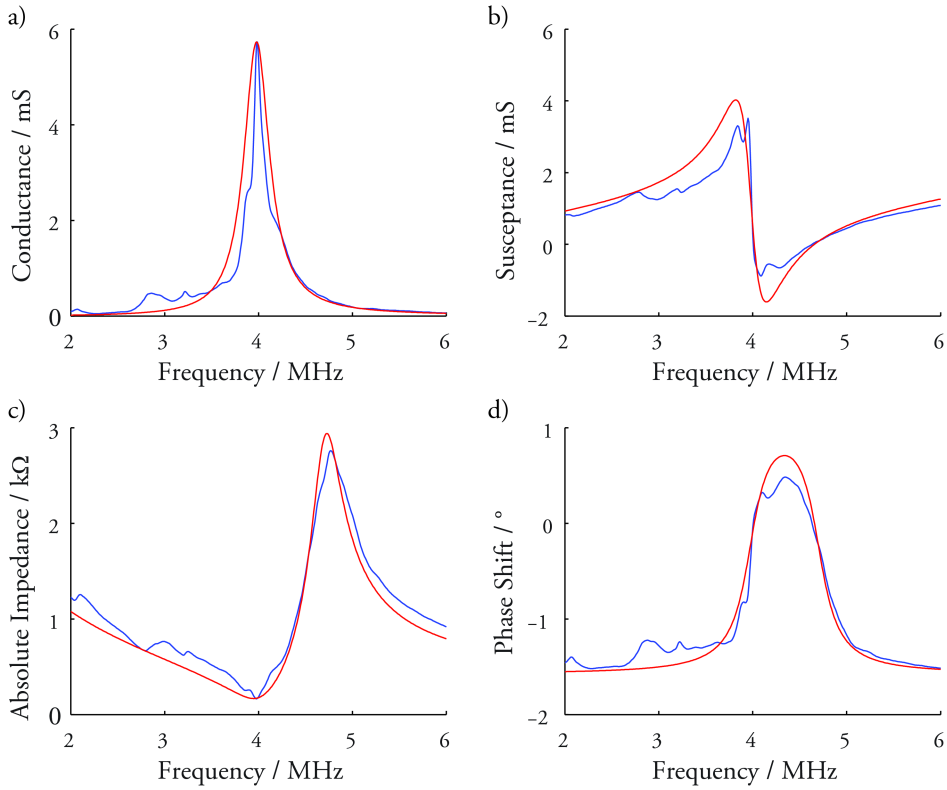

Figure 23: Since the kerfed transducer is dominated by a single resonance-mode it can be effectively modelled as an oscillator circuit. The blue line is the measured data and the red line is calculated from a model using the following values on the circuit elements: R_m = 174.3952 [Ω], L_m = 8.3686e-005 [H], C_m = 1.9108e-011 [F], C_0 = 4.8323e-011 [F], resulting in: f_0 =3980000 [Hz], and Q_m = 12.

The impedance characteristics of the kerfed transducer indicate a 1D resonance that can be modelled with a crystal resonator circuit. The results of this model are shown in **Figure 23** and the values for the circuit elements are given in the figure text. The fact that the piezo can be modelled in this fashion indicates that it is indeed a 1D resonance in the crystal. Analysis of the conductance also allows an estimation of the mechanical Q-value to approximately 12. A Q-value of 12 provides room for improvement, as it is still relatively low, but the proposed model enables a quick way to optimize the mounting procedure without using trapping experiments.

3.2.3 Performance improvements

Coupling the capillary with the transducer has a large impact on the acoustic system resonances. When the two acoustic resonators are coupled the performance of the overall system is heavily influenced by the matching of the two acoustic resonators. For planar devices (i.e. 1D approximation of layered resonators) several design criterions for optimal combinations can be derived [74]. It is suggested here that the fluid layer should have

resonance that is approximately 93 % of the transducer resonance in a low-attenuation system.

The properties of the assembled device can be analysed using impedance measurements. **Figure 24** compares the impedance spectra for a transducer with mounted capillary to the results of a performance benchmark experiment (Paper IV). To benchmark the performance, a cluster of microparticles were captured and the fluid flow was gradually increased until the entire cluster is swept away. Doing this for a number of frequencies allows the maximum retention flow to be plotted as a function of frequency.

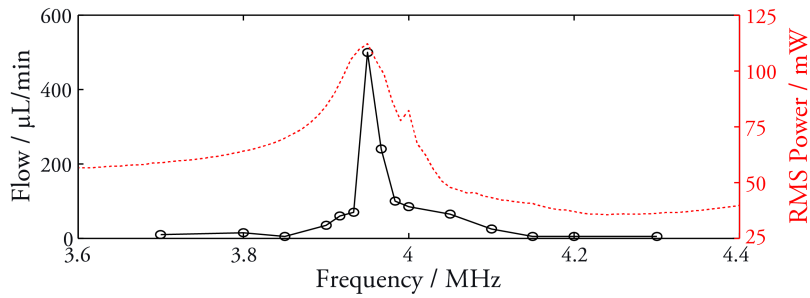

Figure 24: Plotting the delivered root-mean square (RMS) power delivered to the system and the result of a trapping benchmark experiment as function of frequency shows that, for this system, the optimal frequency can be found by selecting the frequency with the most delivered power. As the performance curve is narrower than the power curve one may conclude that this frequency does not only provide the best performance but is also the most effective at using the delivered power.

When comparing the magnitude of the allowed flow rate enabled using the kerfed transducers to that of previously used (Paper I) and closely related systems [36, 80, 81, 160, 161] it is clear that under these conditions the flow rate can be increased approximately one order of magnitude (i.e. from ~10 µL/min to ~100 µL/min). While the performance is to some extent determined by matching, the Q-value and the amount of energy that is bled into spurious modes are also important aspects. As the kerfed transducers have much less of an issue with spurious modes this may in part explain the performance boost.

A challenge that still remains with the trapping systems developed here is variations in performance. To some extent all systems based on resonance suffer from an inherent trade-off between performance and stability. While a high Q-value resonator will utilize the provided energy more efficiently it will also have a narrower frequency-bandwidth, making it more sensitive to changes in the frequency. The matching of the two resonant systems is also a significant source of variation. The used capillaries (VitroCom, NJ, USA) have a size specification of ±10% and there are also variations in the thickness of the PZT-sheets used for fabrication of transducers. Furthermore, although efforts have been made to minimize the complexity of transducer mounting protocol is still introduces some variation. While on the individual resonators (i.e. capillary and transducer) these variations may be less of a problem they do cause problems in the matching of the systems and in turn the performance. In conclusion, some further developments are required to reliably mass-fabricate well-matched systems.

3.2.4 Frequency tracking

By comparing the benchmark experiment to the impedance curve in **Figure 24** one can see that the optimal trapping frequency correlates with the mechanical resonance as measured using impedance. When actuating the piezo with a sine-wave from a function generator the root mean square (RMS) power that is delivered to the system can easily be calculated from the impedance. In Paper IV a setup that uses the fact that the maximum input-power correlates with the optimal frequency for automatic frequency tracking is presented. By using a feedback loop with a frequency update interval of one second an optimal frequency can be maintained. This allows a high Q-value system to be used without sacrificing robustness as changes in temperature and buffer conditions can be compensated for.

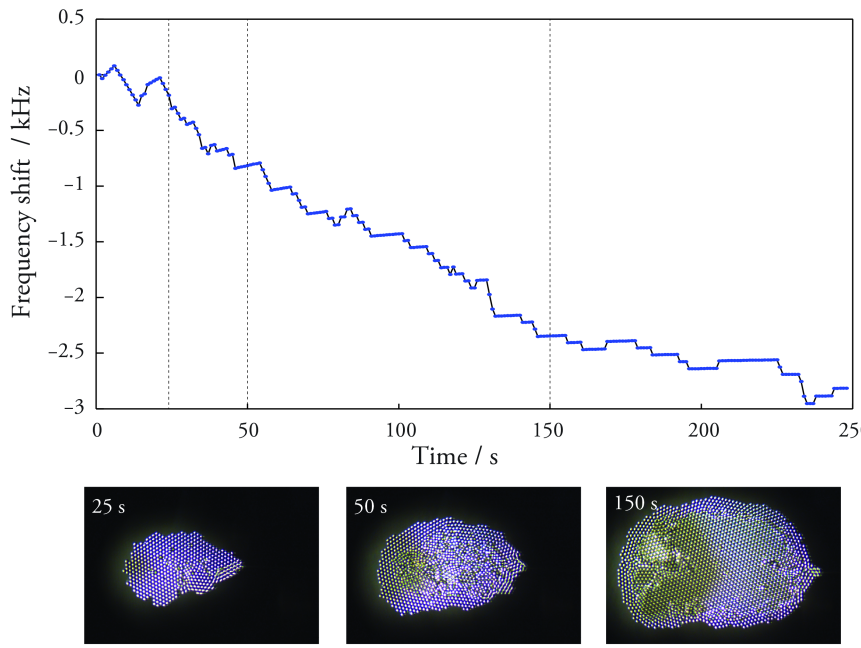

Figure 25: Tracking of the resonance frequency allows changes in the acoustic resonator to be monitored over time. Here, detection of captured particles is made possible by monitoring the frequency decrease as more particles are captured.

While the converse-piezoelectric effect is used to actuate the trap **Figure 25** demonstrates that the piezoelectric effect can be used to measure changes in the trap. As the capillary and transducer are coupled resonators changes in the properties of the capillary can be monitored through the transducer. By analysing electrical properties of the transducer as a function of time, properties such as temperature, buffer conditions, and the amount as well as acoustic properties of captured particles in the trap can be monitored.

3.3 Enabling capture of small particles

As discussed in the acoustofluidics section small particles become increasingly difficult to capture. The highest flow a single particle can be retained at is set by the balance between the trapping force and the fluidic drag. Therefore, if decreasing the particle size at constant flow rate the fluidic drag will eventually supersede the trapping force. This is because the trapping force scales with the volume of the particle whereas the fluidic drag only scales with the radius. Since the acoustic resonator generates acoustic streaming the fluidic drag cannot be decreased below that which is set by the streaming. In the acoustic streaming dominated regime the particles are not captured above the transducer but are instead recirculating in four characteristic streaming rolls as modelled by Lei et al. [144] and demonstrated in **Figure 26**.

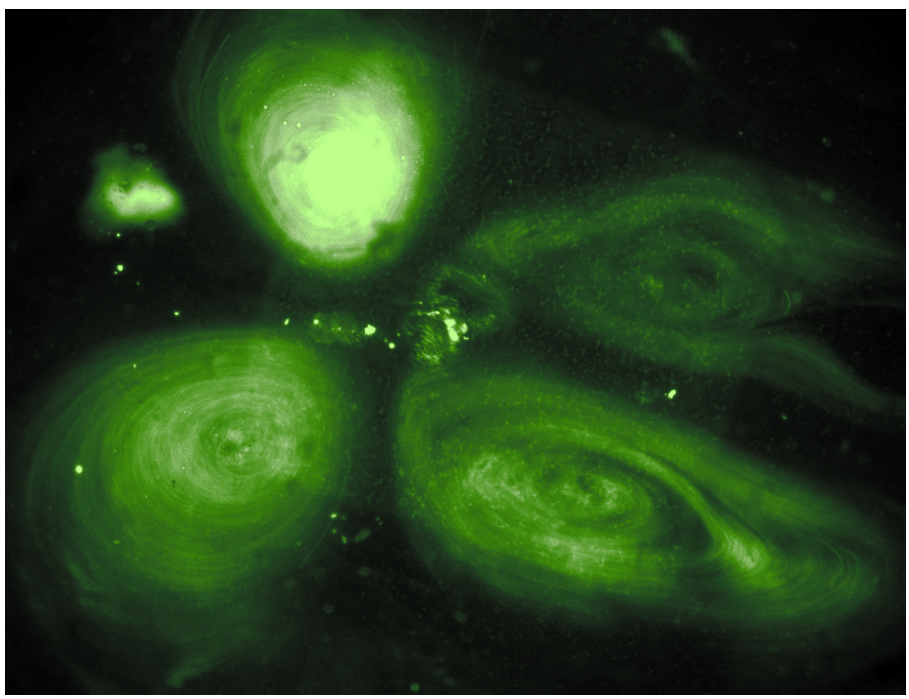

Figure 26: Small particles below the streaming limit are dominated by fluidic drag. The fluorescent 230 nm (diameter) particles seen here are well below this limit, and can be observed in recirculating streaming rolls above the transducer.

The exact size where streaming dominates over trapping force depends on a number of factors, such as the acoustic contrast factors, the resonance frequency, and the viscosity of the fluid. Under typical experimental conditions this transition occurs at particle dimensions around a few micrometres [131, 145, 162]. This is a drawback as the study of sub-micron biological particles often has a high biological relevance. Enabling technology for capture of small particles could for instance allow enrichment, purification, and analysis of

sub-micron particles such as viral particles, sub-cellular organelles, micro-vesicles, as well as certain species of bacteria and fungi.

In Paper II a technique that allows capture of particles with a diameter as low as 110 nm is described. To explain how this is made possible dynamics of capture and retention will be discussed in greater detail.

An experimental observation that is quickly made when using an acoustic trap is that a large group of particles are more easily retained than a single particle. One might anticipate that this is because the acoustic wave doesn't distinguish between two particles in contact and a single larger particle. Conversely when looking at capture, this implies that the first particle will be hardest to capture and as subsequent particles can use the previous particles as a kind of anchor. One might still expect that for non-chemically adherent particles subjected to a fluidic drag detachment would occur and that particles would be gradually lost from the trap.

Experimental work in Paper II showed that even for non-chemically adherent particles (i.e. polystyrene beads in a detergent heavy solution) the particle concentration decides whether trapping or streaming dominates. The results in **Figure 27** show that at sufficiently high concentrations even 500 nm particles began to aggregate above the transducer. One might anticipate that as large groups of particles are brought into close proximity above the transducer the inter-particle scatter would begin to be more and more significant. This could make the secondary acoustic radiation forces significant for agglomeration. The fact that non-chemically adherent particles agglomerate at high concentrations does indeed indicate that particle-particle interaction occur.

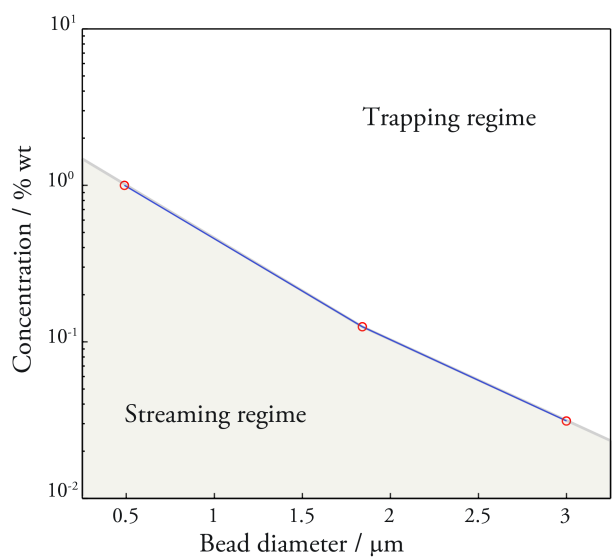

Figure 27: At very high particle concentrations clustering is observed even for particles below the streaming limit, the plotted line is the lowest concentration found to trigger capture for the respective bead size.

As the in-trap concentration and not the global concentration will determine if streaming or trapping dominates, the situation can be easily manipulated by pre-loading the trap with so called seed-particles. **Figure 28** is a demonstration of how trapping of 110 nm particles can be achieved using 10 µm seed-particles to trigger the aggregation. Since this interaction is not chemical, in principle the seed particles can be of arbitrary size or material as long as they can be effectively trapped. When studying the equation for secondary forces more closely one can, however, make some predictions as to which seed-particles may be most effective. Firstly, as the secondary force scales with the volume of both particles large seed-particles should be more effective at capturing small. Secondly, as the second term will be active at longer distances a large compressibility contrast may be highly beneficial. Since the second term increases with the square of the frequency a high frequency would also make these effects more pronounced. In practical applications for enrichment and identification of bacteria presented in thesis 10 µm polystyrene as well as 10 µm silica particles has been utilized successfully.

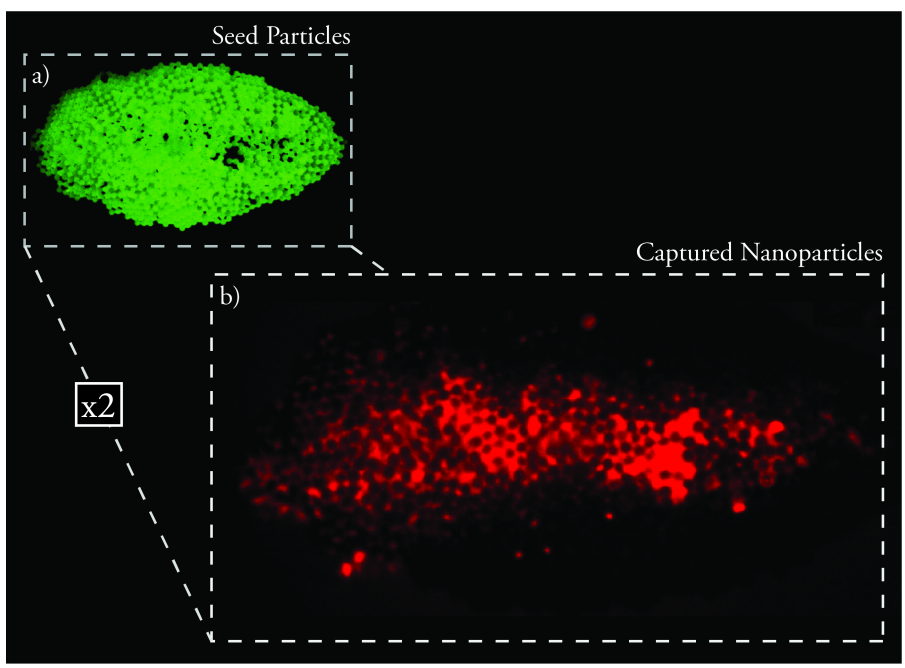

Figure 28: Capture of 110 nm particles (a) is enabled by using 10 µm seed particles (b). The larger seed particles are captured beforehand and interaction with the subsequently introduced nanoparticles allows the streaming limitation to be circumvented.

3.5 Pipette-like integration with MALDI MS

A goal in this thesis has been to integrate the acoustic trap with Matrix Assisted Laser Desorption/Ionization Mass Spectrometry (MALDI MS) to have a fast and label-free

readout. For this to be possible samples have to be extracted from the chip and put into the MALDI-MS bench top instrument. For this reason the acoustic trap has been designed to operate in aspirate/dispense-mode. With a device design as in **Figure 19**, leaving one end of the capillary open and the other end connected to a pump via tubing, the capillary can basically be operated as a pipette with the added feature of particle trapping.

One important feature when utilizing aspirate/dispense is the ability to reverse the direction of the flow without significant delays. Such delays can come from compliance in the system or the construction of the pump. In this work a linear motor syringe pump was used to minimize errors from the pump, as this construction utilizes a feed-back system to control the movement of the piston. To minimize compliance it is important to keep a low fluidic resistance in the tubing between the trap and the pump. This can be done by using tubing with large inner-diameter (such as 0.8 mm).

Applying a hydrophobic surface treatment to the exterior of the capillary with allows small volumes to be more easily deposited onto a MALDI MS-target. In standard dried-droplet MALDI MS, a single spot on the standard target can hold approximately 2 μL of liquid (depending on surface tension). By repeatedly depositing samples on different spots during perfusion of a trapped cluster a time resolved measurement is enabled. The volume in each collected aliquot multiplied with the flow rate determines the discrete steps of the time resolution. This means that by collecting larger samples the sensitivity can be increased at the expense of the time resolution. In principle several droplets could be deposited on the same target, however, this is very time consuming as one have to wait for evaporation of the previous droplet and there are also issues with salts accumulating on the target spot which has a detrimental effect on the sensitivity.

Solid phase extraction (SPE) is a sample preparation method that allows enrichment and separations of analytes via interaction with a solid matrix. SPE can be performed with microbeads utilizing chemical interactions such as ion exchange or polarity via so called reverse phase (RP) beads. Using SPE for the aliquots collected from trapped particles allow analytes from a larger fluid volume to be accumulated without simultaneously increasing the salt concentration. In this work samples were deposited into an Integrated Selective Enrichment Target (ISET) chip. The ISET chip was developed by Ekström et al. [163], and it consists of a silicon target with perforated vials where SP beads can be loaded. The fact that any beads can be loaded and that samples can be directly deposited in the ISET microchip made it a more practical choice than commercially available formats such as ZipTip®. In conclusion, a SP step was included in the system to allow a generic aliquot volume to be analysed and to provide a sometimes needed boost to sensitivity

Obviously a trapping device operated in aspirate/dispense mode can automated just like a pipetting robot. This has been done by mounting the device in a XYZ-stage capable of moving the open tip between different wells in a microtiter plate, an overview of the automated system is given in **Figure 29**. Computer control of both the pump and the stage (LabVIEW, National Instruments, TX, USA) allowed arbitrary experimental protocols to be automated.

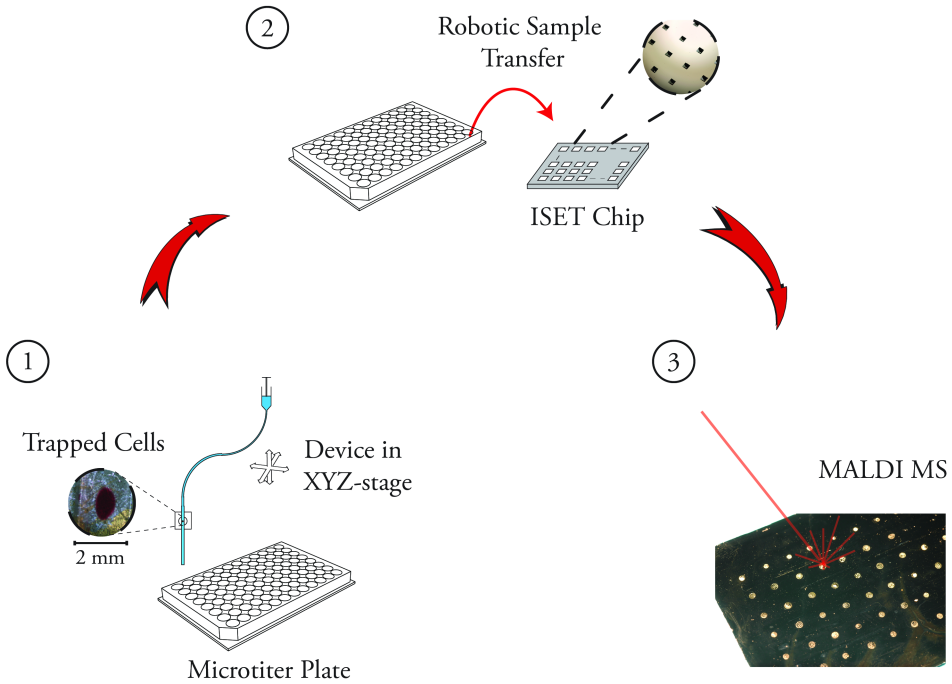

Figure 29: The workflow for providing automated sample preparation and MALDI MS readout from the acoustic trap. Assay steps can be performed on a trapped cluster via aspirate/dispense from a microtitreplate (1), and deposition of aliquots into an ISET chip (2) allows time traceable MS analysis (3).

4 Biomedical applications

4.1 Automated sample preparation for bead-based assays

Affinity extraction protocols using magnetic microparticles with immobilized antibodies are common practice. One instance where affinity bead extraction is used is in immuno-MALDI MS, where an affinity extraction is followed by a mass spectrometric readout. This method can have some advantages over a standard ELISA-assay as there is room for discovery of cross-reacting species and structural variants of the antigen can be identified[164, 165]. It is believed that similar use of mass spectrometry is a promising way forward in clinical diagnosis[166, 167, 168, 169] and can provide new means for personalized medicine[170, 171].

Application of the acoustic trapping pipette to immuno-MALDI MS identification of a peptide hormone in plasma is demonstrated in Paper III. Here, angiotensin I specific microparticles was used to extract the peptide from plasma samples.

The standard protocol for doing this is based on particle manipulation using magnetic beads. This protocol uses detergents for bead-solubility; a needed precaution to prevent beads form sticking to surfaces in test tubes and pipette tips. This is a problem since detergents interfere with the MALDI MS readout by creating a ladder of peaks. The spectra in **Figure 30**a shows this background ladder after three magnetic bead washing steps (according to the manufacturer's specification). In summary, the use of detergents creates an unwanted trade-off between removing background interference and preventing bead-loss.

Non-contact trapping allows that measurable detergent levels can be washed away from the sample without risk of losing beads due to surface contact. By aspirating a non-detergent buffer solution and allowing it to perfuse the trapped particles, three manual washing steps can be substituted by a single step. In addition, a more efficient detergent removal as shown by the spectra in **Figure 30**b is achieved. The affinity extraction protocol can also be automated in the robotic trapping pipette setup in **Figure 29**.

An interesting observation during the work with this assay was that when using the acoustic trap identical results was obtained when using a 5 minute sample incubation time as when using the 1 hour incubation needed for the standard assay. This showcases one of the benefits of having short diffusion distances in a microfluidic format but is also probably influenced by the acoustic streaming that provides active mixing of the liquid. As a final note on trapping of functionalized particles, one might add removing the need for magnetic properties allows a greater freedom in selecting the bead-material. Whether this can be used

to manufacture cheaper or more effective beads, by e.g. making them porous, remains to be seen.

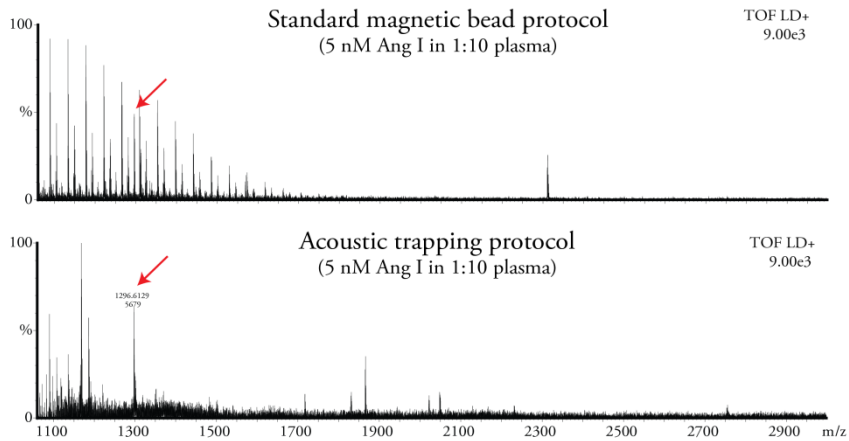

Figure 30: Non-contact acoustic trapping of microparticles provide an attractive alternative to standard magnetic beads by allowing increased washing efficiency and assay speed. The top spectra is obtained from a standard magnetic bead protocol and the lower spectra is obtained through acoustic trapping, comparing these shows efficient removal of the interference from the used detergents (seen as a ladder of equidistant peaks).

4.2 A platform for dynamic cell studies

The fact that cells can remain viable in the acoustic trap provides an interesting opportunity to study the activity of a small trapped population of cells. Retaining a small population of cells against a fluid flow provides a straightforward way to continuously separate intracellular and extracellular substances.

A demonstration of how the localization of drug-molecules can be analysed using the setup [172] is provided in **Figure 31**. Here, a population of cells are captured from blood containing a known membrane binder and an impermeable peptide. Washing with PBS and collecting two fractions allows proteins in the plasma to be found in the first fraction and the successful removal of them can be confirmed in the second fraction. Aspirating a lysis buffer subsequently allows the content of the cells to be addressed. When comparing the lysed fraction to the other two many differential peaks are observed, indicating the potential to access not only the localization but also the effects of different substances.

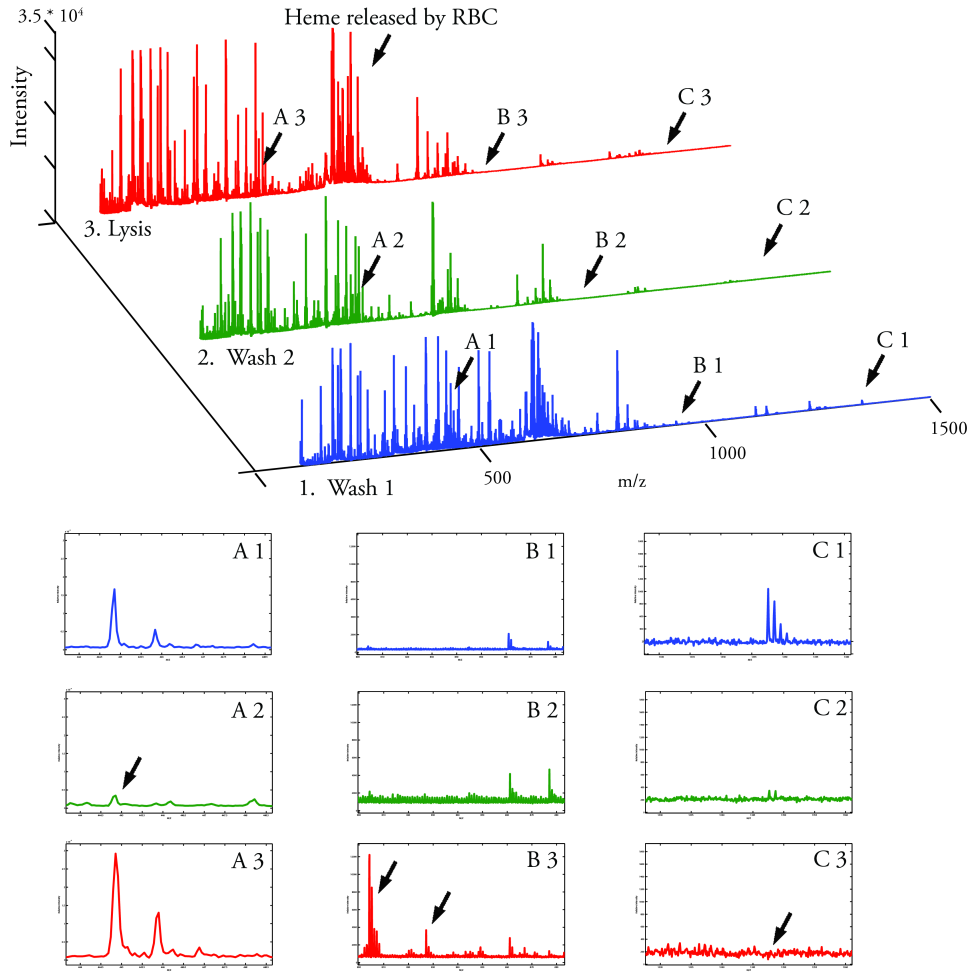

Figure 31: This experiment demonstrates how analysing fractions taken during the course of an experiment enables analysis of drug-uptake. In this case a blood sample is analysed showing that it is possible to determine whether the cells have incorporated the spiked drugs or not. Analysis of three fractions was performed and three arrows denote areas of interest that are enlarged below the spectra. The blue trace shows the first wash containing excess blood cells, debris and plasma. The green trace shows the second wash fraction containing traces of plasma, surface bound species and cellular leakage. The red trace, shows the spectra resulting from lysis of the trapped RBC, successful lysis is here confirmed by the strong increase of signals from released Heme groups observed just above 600Da. The first area of interest (A) shows the peak of a drug spiked in the sample, this peak disappears in the second fraction and reappears in the third confirming uptake of the drug. The second area of interest (B) shows an enlargement of differential peaks specific to the lysed fraction, demonstrating that peptide/metabolite localization can be facilitated by the system. The third area of interest (C) shows the peak of a spiked peptide (1347 Da) spiked in the sample, the absence in spectra C3 confirms that this peptide cannot penetrate the cell membrane.

As can be seen in the spectrums the lysed blood population constitutes a rather complex sample with many peaks. To demonstrate that, in spite of this, specific analytes can be found a blood sample was incubated with fluoxetine, a well-known selective serotonin reuptake inhibitor drug. Capturing and washing cells from this sample showed that the drug molecule could indeed be found among the cells, **Figure 32**. Here, a MALDI MS Orbitrap instrument was used as this allows an excellent mass-resolution which is helpful when identifying a single peak in such complex sample. To ensure that the peak represented the fluoxetine both spiking of a D5 isotope and MS/MS was used. Furthermore, adding a known amount of isotope to the target demonstrates how the amount of analyte can be quantified by comparing peak-heights.

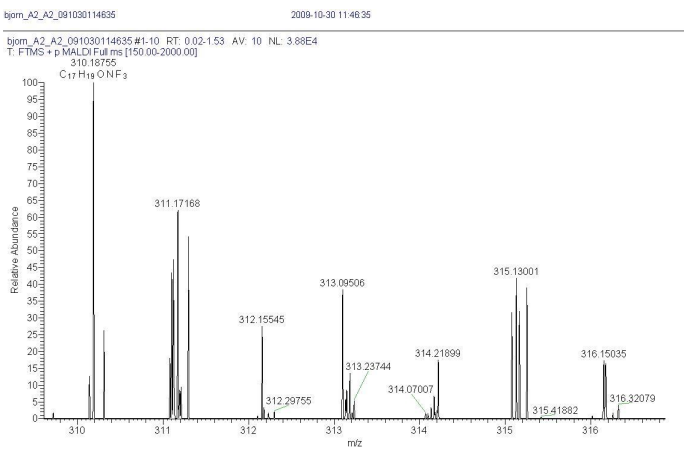

Figure 32: Identification of fluoxetine ($C_{17}H_{19}ONF_3$) from lysed cell population using a high mass resolution MALDI MS instrument. The possibility of quantification of the uptake is demonstrated by addition of a known amount of D5 isotope (found 5 Da above the fluoxetine peak).

As previously mentioned the time resolved MS readout can be one advantage of this platform, but also when combined with analysis of the resonance frequency it can provide means to monitor the size and composition of the cell population. With further studies, there may also be potential for improved studies of non-adherent cells such as platelets and white blood cells by utilizing the non-contact handling to provide a more *in vivo* like environment.

4.3 Purification of bacteria from infected blood samples

Seed particles allow capture of small particles at low concentrations below the streaming limitation. This principle enables capture of bacteria as shown in **Figure 33**. In Paper II it was shown that the capture efficiency for Escherichia coli in a saline solution is dependent on flow rate. Here, 95 % capture efficiency could be obtained if the flow rate is low (in this case 10 µL/min). Interestingly, if the flow rate is increased (up to 90 µL/min) the capture

efficiency drops off but this is compensated by a greater influx of bacteria such that the capture rate (i.e. bacteria capture per second) is greater.

Similar capture of bacteria is potentially useful for purification of microbes from complex samples. In clinical microbiology, a wide range of different samples are routinely handled including, blood, urine, cerebrospinal fluid, sputum, and stool-specimens. Furthermore, MALDI MS is rapidly becoming a standard method of detecting and typing bacteria and fungi in such settings [18]. However, before detection and typing can be accomplished in such complex samples manual sample preparation is required. This sample preparation has been identified as a general concern [173] making diagnosis unnecessarily time consuming and costly.

Paper V investigates the possibility of using the acoustic trap to replace the manual sample preparation needed for bacteria typing in blood samples – a necessary component in diagnosis of bacteraemia induced sepsis. The standard method for doing this is to use a centrifugation-based protocol that lyses the blood cells allowing the bacteria to be pelleted and washed with a total of three centrifugation steps. The time used for this protocol is obviously dependent on the operator but a reported value for the assay is 40 minutes [174] while the manufacturer estimates it to 30 minutes [175].

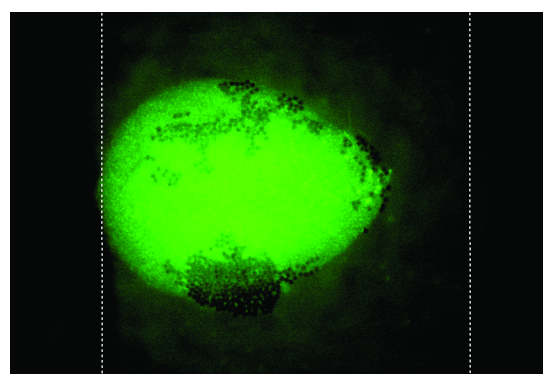

Figure 33: Micrograph of captured E. coli coloured with a green live stain. The outlines of the transducer are dashed in white and the 10 μm seed-particles are seen as dark patterns in the cluster.

This protocol can also be performed in an acoustic trap by capturing bacteria from a lysed solution and subsequently aspirating water, followed by a formic acid lysis of the captured bacteria. Using the automated workflow described in **Figure 29** this was shown for E. coli infected blood samples. For twelve out of twelve samples the correct species were identified against the used BioTyper database. Comparing the obtained score-values (i.e. a metric of the security of the identification) the acoustic protocol slightly outperformed the manual assay with an average score of 2.19±0.09, as compared to 1.98±0.08 when using the manual protocol for the same strain. Apart from a slight improvement in score values the primary gain is here that the sample preparation could be performed in 5-6 minutes in a way that can be automated using standard laboratory robotics.

The challenge with adapting the used protocol to the acoustic trapping platform has been to handle the large differences in viscosity and acoustic properties (i.e. density and compressibility) between the used liquids. For instance the different properties of the lysed blood and the deionized water required adjustment of the actuation frequency, something that was enabled by the resonance frequency tracking method (section 3.2.4).

For future applications, it is interesting to note that the live stain used to show E. coli in **Figure 33** in combination with previous studies [114] suggest that bacteria can remain viable in the acoustic trap. This may allow more advanced studies, such as were conducted on blood cells (section 4.2), to be conducted on captured bacteria leaving some room for future developments to address major challenges such as quickly assessing antibiotics resistance or providing new tools for strain-typing.

Populärvetenskaplig sammanfattning

I naturen finns en närmast oändlig variation av biologiska partiklar i storleksordningen 100 nanometer till 10 mikrometer. Bland dessa kan man bland annat finna; eukaryota celler som genom ordnad samverkan bygger upp flercelliga organismer, prokaryota celler vilka lever som solitära organismer såsom olika bakterier eller jästsvamp, och viruspartiklar vilka likt parasiter specialiserat sig på att få större celler att reproducera deras DNA. De flesta av dessa partiklar lever i vätska och vår förståelse för hur de fungerar och interagerar med varandra är avgörande för hur vi diagnosticerar och behandlar en mängd sjukdomar, men också för hur vi ser på vår omvärld.

På mikro- och nanoskalan bestäms vilken information vi har att tillgå av de tekniska hjälpmedel som finns till hands. En stor utmaning är även att levande organismer hela tiden interagerar med sin omgivning och det är därför viktigt att så gott det går försöka återskapa den miljö som man vill studera dem i.

En relativt ny utveckling inom detta område är att använda sig av avancerade mikrofabrikationsmetoder som återfinns i halvledarindustrin för att i stället göra små mikrosystem för kemisk och biologisk analys. Här används nätverk av tunna vätskekanaler för att transportera och blanda reagens och prover. I många fall ger detta möjligheter till nya och bättre kontrollerade experiment och tillåter att man utför dem på ett snabbt och automatiserat sätt. I denna typ av mikro-laboratorier behövs dock ofta ett sätt att hålla fast och positionera de små biologiska partiklar man vill studera. Denna avhandling beskriver just en sådan metod där man använder ultraljud för att skapa en partikelfälla, som kan samla upp och hålla kvar celler i vätska utan att vidröra dem.

Fundamentalt är en ljudvåg mikroskopiska vibrationer och om vibrationsfrekvensen är ovanför det hörbara området klassificeras den som en ultraljudsvåg. Vid så höga frekvenser blir ljudets våglängd så kort att man kan skapa resonanser i en mikrokanal. Detta fenomen liknar på många sätt hur särskilda toner/frekvenser förstärks i ett musikaliskt instrument beroende på dess dimensioner. I vilket fall tillåter detta att de små vibrationerna förstärks tillräckligt för att man ska kunna påverka olika partiklars position.

Genom att designa ljudfältet så att intensiteten är särskilt hög i en specifik punkt kan en så kallad akustisk partikelfälla åstadkommas. Detta kan man praktiskt åstadkomma genom att använda en liten ljudkälla (i from av ett piezoelektriskt element) för att lokalt driva en resonans i ett litet vätskefyllt glasrör.

Inom ramen för avhandlingen beskrivs metoder för att realisera en akustisk partikelfälla på ett effektivt och enkelt sätt, men även teknisk utveckling som möjliggjort applikationer inom biomedicinteknik. Exempelvis har en ny metod utvecklats för att fånga mindre

partiklar än vad som tidigare var möjligt med ultraljud. I samarbete med avdelningen för klinisk mikrobiologi i Lund har denna teknik i sin tur använts för att samla upp och artbestämma bakterier från blodprover. Detta är ett viktigt steg i diagnostisering av blodförgiftning, eller sepsis, som är ett akut tillstånd där man snabbt vill avgöra om och i så fall vilken bakterieinfektion som är orsaken. Här tillåter den akustiska fällan att man på ett snabbt och automatserat sätt gör en nödvändig upprening av bakterierna, en process som annars spiller dyrbar tid och resurser hos de kliniska laboratorierna.

I vilken mån den teknologi som beskrivs här kan komma att användas för att tackla stora samhällsutmaningar såsom spridning av resistenta bakterier eller de i västvärlden dramatiskt ökande vårdkostnaderna får framtiden utvisa. Men det står klart att en fortsatt teknisk utveckling är nödvändig för att hålla jämna steg med de nya utmaningar som mikroorganismerna ställer oss inför.

Acknowledgements

There are many people who have helped me during my time at department, and who deserve to be thanked. There has been a good atmosphere, where people are helpful and where new ideas can be openly discussed. This has been crucial for me to succeed with many of the things I wanted to accomplish during my PhD.

Firstly, I want to thank Johan, my supervisor, who gave me the opportunity to work at the department after my master thesis. It has been very important for me to have a dependable person who I have been able to have in-depth discussions on how the device actually works with. Most of all I greatly appreciate the confidence you have shown me, and the fact that I have been allowed to influence the direction of the research and pursue new ideas.

I also want to thank my assistant supervisor Thomas for creating a good research environment. Over the years we have had several great research discussions which have been very helpful, and your positive attitude has been very motivating. Two specific things I would like to thank for is the opportunity to write a review early in the PhD, and your help in outlining the seeding paper which helped me to better structure the rest of my papers.

Next on the thank you-list are obviously Simon and Mikael who both have been indispensable both as friends and as fellow researchers.

My collaboration with Simon started at a crayfish party shortly after I got hired at the department. We then decided to initiate a skunk-work project where we combined his maldi-thing with the trap. Pretty soon thereafter we got an oral presentation at μTAS where a nervous rookie had to present in front of close to 500 people in Korea. To me this is a great example of the kind of opportunity that can come up in a good research environment (and also of having enough freedom to pursue it). Since then we have worked on several official projects together and I have learned a lot from you. The help with retaining mental sanity during long and stressful times through after-work activities such as StarCraft and BarCraft have also been epic.

My former master-thesis supervisor Mikael has continuously worked with me on improving the device since he came back from Stanford. This has been a huge benefit for me as many innovative ideas and solutions have come out of our discussions together. Thank you for this and also for being an intense e-mailer, and always having new side-projects like baking with sour dough or building home-made acoustic guitars.

I also want to thank all of my current and former colleagues at elmät/bme both for practical help and for great memories. Some specific thanks goes out to: Andreas for carrying the acoustics meetings and conserving hit-points in wot. Per for realizing the awesomeness of both pneumatics and SPÖK-pneumatics. Calle for wot-carry and epic conference

memories. Pelle for always being able to find a more difficult perspective. Christian for making a norrlänning feel less like a skåning. Martin for being nice enough not to beat my wn8-score yet. Axel for pro bono matlab-scripts and in-depth lessons in Japanese history. Ola for saving me from drifting to Denmark. Sameer for keeping in touch from Poland. Fredrik for discussions on good places for downhill-skiing and computer aid. Klara for also escaping the infamous German-snus-incident. Kishore for liberal use of Indian spice mixes. Maria N for being a great researcher and winning the lab-bench complexity challenge. John for providing necessary breaks from the computer where furniture is moved or cookies are eaten. Belinda for parallel graduation. Maria T for picking up acoustic trapping scaringly fast. Hans for always finding time to discuss my many questions and highlighting the complexity of the world. The entire ultrasound group and particularly Hans, Tomas and Magnus for being very helpful, and making a great PhD-course. Without the discussions with you guys, I would probably not have started using kerfed transducers. Désirée for being extremely helpful in showing me how to jump through the hoops associated with graduation.

I want to acknowledge my collaborators: Hong Yan for her work on the affinity trapping paper. Bo Nilson for his insights in the practices of clinical microbiology, guiding us around among the scary microbes in the lab, and providing us with relevant samples to analyse. I want to thank Brian Poe and professor James Landers from UVA in Charlottesville for taking the initiative to come over seas to visit our lab and start collaboration. Best of luck to you guys!

My master thesis students Herve Barbeau and Jacob Whalström, you deserve many thanks for your ambitious work in the lab and best of luck to you both in the future!

The financial support from The Swedish Research Council, The Crafoord Foundation, Knut och Allice Wallenberg, Sigfrid och Walborg Nordkvist Foundation and Kungliga Fysiografiska Sällskapet is greatly acknowledged. Without your investments in our projects the made progress would not have been possible. I sincerely hope that you find the results of interest, thank you.

Most of all, I would like to thank my family. Thanks to my parents for being very supportive and always showing a great interest in my work (to Stene for proofreading the entire dissertation). Thanks to my dear Sofia for being with me every day and for your support, care and advice. I promise I will try to return the favours when you graduate.

References

1. H. Gest, Notes and records of the Royal Society of London **58** (2), 187-201 (2004).
2. E. R. Mardis, Nature **470** (7333), 198-203 (2011).
3. M. L. Metzker, Nat Rev Genet **11** (1), 31-46 (2010).
4. E. Neher and B. Sakmann, Nature **260** (5554), 799-802 (1976).
5. O. P. Hamill, A. Marty, E. Neher, B. Sakmann and F. J. Sigworth, Pflügers Archiv European Journal of Physiology **391** (2), 85-100 (1981).
6. A. Manz, N. Graber and H. M. Widmer, Sensor Actuat B-Chem **1** (1-6), 244-248 (1990).
7. G. M. Whitesides, Nature **442** (7101), 368-373 (2006).
8. A. R. Wheeler, W. R. Throndset, R. J. Whelan, A. M. Leach, R. N. Zare, Y. H. Liao, K. Farrell, I. D. Manger and A. Daridon, Anal Chem **75** (14), 3581-3586 (2003).
9. D. B. Weibel and G. M. Whitesides, Current Opinion in Chemical Biology **10** (6), 584-591 (2006).
10. J. Melin and S. R. Quake, Annu Rev Bioph Biom **36**, 213-231 (2007).
11. E. Verpoorte, Electrophoresis **23** (5), 677-712 (2002).
12. A. J. Tudos, G. A. J. Besselink and R. B. M. Schasfoort, Lab Chip **1** (2), 83-95 (2001).
13. Beards, B. (October 21, 2008). *Electron micrograph of Bacteriophages*. In Wikimedia Commons. Retrieved April 7, 2014, from http://en.wikipedia.org/wiki/File:Phage.jpg.
14. National Institutes of Health. (December 7, 2005). *Color-enhanced scanning electron micrograph showing Salmonella typhimurium (red) invading cultured human cells*. In Wikimedia Commons. Retrieved April 7, 2014, from http://en.wikipedia.org/wiki/File:SalmonellaNIAID.jpg.
15. D. Huh, G. A. Hamilton and D. E. Ingber, Trends in Cell Biology **21** (12), 745-754 (2011).
16. J. van der Greef and R. N. McBurney, Nat Rev Drug Discov **4** (12), 961-967 (2005).
17. J. El-Ali, P. K. Sorger and K. F. Jensen, Nature **442** (7101), 403-411 (2006).
18. A. E. Clark, E. J. Kaleta, A. Arora and D. M. Wolk, Clin Microbiol Rev **26** (3), 547-603 (2013).
19. C. Dong and X. X. Lei, J Biomech **33** (1), 35-43 (2000).
20. J. Cao, S. Usami and C. Dong, Ann Biomed Eng **25** (3), 573-580 (1997).
21. C. Piggee, Anal Chem **81** (1), 16-19 (2009).
22. A. N. Grigorenko, N. W. Roberts, M. R. Dickinson and Y. Zhang, Nature Nanotechnology **2** (6), 365-370 (2008).
23. D. G. Grier, Nature **424** (6950), 810-816 (2003).
24. J. Voldman, M. Toner, M. L. Gray and M. A. Schmidt, J. Electrost. **57** (1), 69-90 (2003).
25. B. M. Taff and J. Voldman, Anal Chem **77** (24), 7976-7983 (2005).
26. M. A. M. Gijs, Microfluid. Nanofluid. **1** (1), 22-40 (2004).
27. A. Winkleman, K. L. Gudiksen, D. Ryan, G. M. Whitesides, D. Greenfield and M. Prentiss, Appl. Phys. Lett. **85** (12), 2411-2413 (2004).

28. E. Mirowski, J. Moreland, A. Zhang, S. E. Russek and M. J. Donahue, Appl. Phys. Lett. **86** (24), 3 (2005).
29. H. Lee, A. M. Purdon and R. M. Westervelt, Appl. Phys. Lett. **85** (6), 1063-1065 (2004).
30. Q. Ramadan, V. Samper, D. Poenar and C. Yu, Biomed. Microdevices **8** (2), 151-158 (2006).
31. Q. Ramadan, V. Samper, D. P. Poenar and C. Yu, Biosens. Bioelectron. **21** (9), 1693-1702 (2006).
32. T. R. Strick, J. F. Allemand, D. Bensimon, A. Bensimon and V. Croquette, Science **271** (5257), 1835-1837 (1996).
33. C. Gosse and V. Croquette, Biophys. J. **82** (6), 3314-3329 (2002).
34. A. H. B. de Vries, J. S. Kanger, B. E. Krenn and R. van Driel, J. Microelectromech. Syst. **13** (3), 391-395 (2004).
35. A. H. B. de Vries, B. E. Krenn, R. van Driel and J. S. Kanger, Biophys. J. **88** (3), 2137-2144 (2005).
36. M. Evander, L. Johansson, T. Lilliehorn, J. Piskur, M. Lindvall, S. Johansson, M. Almqvist, T. Laurell and J. Nilsson, Anal Chem **79** (7), 2984-2991 (2007).
37. M. Wiklund, S. Nilsson and H. M. Hertz, J. Appl. Phys. **90** (1), 421-426 (2001).
38. M. Wiklund and H. M. Hertz, Lab Chip **6** (10), 1279-1292 (2006).
39. M. Wiklund, C. Gunther, R. Lemor, M. Jager, G. Fuhr and H. M. Hertz, Lab Chip **6** (12), 1537-1544 (2006).
40. A. Ashkin, Phys Rev Lett **24** (4), 156-& (1970).
41. Y. Arai, R. Yasuda, K. Akashi, Y. Harada, H. Miyata, K. Kinosita and H. Itoh, Nature **399** (6735), 446-448 (1999).
42. K. Mangold, P. Leiderer and C. Bechinger, Phys Rev Lett **90** (15) (2003).
43. H. A. Pohl, J. Appl. Phys. **22** (7), 869-871 (1951).
44. P. Singh and N. Aubry, Phys Rev E **72** (1) (2005).
45. B. H. Lapizco-Encinas, B. A. Simmons, E. B. Cummings and Y. Fintschenko, Anal Chem **76** (6), 1571-1579 (2004).
46. M. S. Yang, C. W. Li and J. Yang, Anal Chem **74** (16), 3991-4001 (2002).
47. D. Di Carlo, N. Aghdam and L. P. Lee, Anal Chem **78** (14), 4925-4930 (2006).
48. A. M. Skelley, O. Kirak, H. Suh, R. Jaenisch and J. Voldman, Nat Meth **6** (2), 147-152 (2009).
49. B. R. Lutz, J. Chen and D. T. Schwartz, Anal Chem **78** (15), 5429-5435 (2006).
50. B. R. Lutz, J. Chen and D. T. Schwartz, P Natl Acad Sci USA **100** (8), 4395-4398 (2003).
51. J.-C. Eric M, T. Melikhan and S. Charles M, Journal of Visualized Experiments (47) (2011).
52. M. Tanyeri, M. Ranka, N. Sittipolkul and C. M. Schroeder, Lab Chip **11** (10), 1786-1794 (2011).
53. A. Kundt, Annalen der Physik **203** (4), 497-523 (1866).
54. M. Dyson, B. Woodward and J. B. Pond, Nature **232** (5312), 572-& (1971).
55. N. V. Baker, Nature **239** (5372), 398-& (1972).
56. E. G. Lierke, Acustica **82** (2), 220-237 (1996).
57. T. Laurell, F. Petersson and A. Nilsson, Chem Soc Rev **36** (3), 492-506 (2007).
58. A. Lenshof and T. Laurell, Chem Soc Rev **39** (3), 1203-1217 (2010).
59. W. T. Coakley, D. W. Bardsley, M. A. Grundy, F. Zamani and D. J. Clarke, J. Chem. Technol. Biotechnol. **44** (1), 43-62 (1989).

60. H. M. Hertz, J. Appl. Phys. **78** (8), 4845-4849 (1995).
61. M. A. Grundy, W. E. Bolek, W. T. Coakley and E. Benes, J Immunol Methods **165** (1), 47-57 (1993).
62. L. A. Kuznetsova and W. T. Coakley, Biosens. Bioelectron. **22** (8), 1567-1577 (2007).
63. R. W. Ellis and M. A. Sobanski, J. Med. Microbiol. **49** (10), 853-859 (2000).
64. M. Wiklund, Lab Chip **12** (11), 2018-2028 (2012).
65. M. Wiklund, J. Toivonen, M. Tirri, P. Hanninen and H. M. Hertz, J. Appl. Phys. **96** (2), 1242-1248 (2004).
66. L. Gherardini, C. M. Cousins, J. J. Hawkes, J. Spengler, S. Radel, H. Lawler, B. Devcic-Kuhar and M. Groschl, Ultrasound Med. Biol. **31** (2), 261-272 (2005).
67. D. Bazou, W. T. Coakley, A. J. Hayes and S. K. Jackson, Toxicology in Vitro **22** (5), 1321-1331 (2008).
68. J. Hultstrom, O. Manneberg, K. Dopf, H. M. Hertz, H. Brismar and M. Wiklund, Ultrasound Med. Biol. **33** (1), 145-151 (2007).
69. G. E. Kaufman, M. W. Miller, T. Dan Griffiths, V. Ciaravino and E. L. Carstensen, Ultrasound in Medicine & Biology **3** (1), 21-25 (1977).
70. C. R. Hill, J Acoust Soc Am **50** (1), 90-& (1971).
71. J. W. Ellwart, H. Brettel and L. O. Kober, Ultrasound in Medicine & Biology **14** (1), 43-50 (1988).
72. D. Carugo, D. N. Ankrett, P. Glynne-Jones, L. Capretto, R. J. Boltryk, P. A. Townsend, X. Zhang and M. Hill, Biomicrofluidics **5** (4), 044108 (2011).
73. J. Liu, T. N. Lewis and M. R. Prausnitz, Pharmaceut Res **15** (6), 918-924 (1998).
74. P. Glynne-Jones, R. J. Boltryk and M. Hill, Lab Chip **12** (8), 1417-1426 (2012).
75. S. M. Woodside, B. D. Bowen and J. M. Piret, Aiche J **43** (7), 1727-1736 (1997).
76. D. Bazou, L. A. Kuznetsova and W. T. Coakley, Ultrasound Med. Biol. **31** (3), 423-430 (2005).
77. J. Liu, L. A. Kuznetsova, G. O. Edwards, J. S. Xu, M. W. Ma, W. M. Purcell, S. K. Jackson and W. T. Coakley, Journal of Cellular Biochemistry **102** (5), 1180-1189 (2007).
78. D. Bazou, E. J. Blain and W. T. Coakley, Molecular Membrane Biology **25** (2), 102-U116 (2008).
79. G. O. Edwards, D. Bazou, L. A. Kuznetsova and W. T. Coakley, Toxicology **231** (2-3), 101-102 (2007).
80. T. Lilliehorn, U. Simu, M. Nilsson, M. Almqvist, T. Stepinski, T. Laurell, J. Nilsson and S. Johansson, Ultrasonics **43** (5), 293-303 (2005).
81. T. Lilliehorn, M. Nilsson, U. Simu, S. Johansson, M. Almqvist, J. Nilsson and T. Laurell, Sensor Actuat B-Chem **106** (2), 851-858 (2005).
82. W. W. Hansen, J. Appl. Phys. **9** (10), 654-663 (1938).
83. F. E. Terman, *Electronic and Radio Engineering*. (McGraw-Hill, 1955).
84. O. Manneberg, B. Vanherberghen, J. Svennebring, H. M. Hertz, B. Onfelt and M. Wiklund, Appl. Phys. Lett. **93** (6) (2008).
85. O. Manneberg, J. Svennebring, H. M. Hertz and M. Wiklund, J Micromech Microeng **18** (9) (2008).
86. B. Vanherberghen, O. Manneberg, A. Christakou, T. Frisk, M. Ohlin, H. M. Hertz, B. Onfelt and M. Wiklund, Lab Chip **10** (20), 2727-2732 (2010).
87. A. E. Christakou, M. Ohlin, B. Vanherberghen, M. A. Khorshidi, N. Kadri, T. Frisk, M. Wiklund and B. Onfelt, Integr Biol-Uk **5** (4), 712-719 (2013).

88. S. Oberti, A. Neild and J. Dual, J Acoust Soc Am **121** (2), 778-785 (2007).
89. X. Y. Ding, S. C. S. Lin, B. Kiraly, H. J. Yue, S. X. Li, I. K. Chiang, J. J. Shi, S. J. Benkovic and T. J. Huang, P Natl Acad Sci USA **109** (28), 11105-11109 (2012).
90. G. Destgeer, K. H. Lee, J. H. Jung, A. Alazzam and H. J. Sung, Lab Chip **13** (21), 4210-4216 (2013).
91. J. Lee, S.-Y. Teh, A. Lee, H. H. Kim, C. Lee and K. K. Shung, Appl. Phys. Lett. **95** (7), 073701 (2009).
92. J. Hu, J. Xu, J. Yang, J. Du, Y. Cai and C. Tay, Ultrasonics, Ferroelectrics and Frequency Control, IEEE Transactions on **53** (3), 571-578 (2006).
93. H. Bruus, J. Dual, J. Hawkes, M. Hill, T. Laurell, J. Nilsson, S. Radel, S. Sadhal and M. Wiklund, Lab Chip **11** (21), 3579-3580 (2011).
94. H. Bruus, Lab Chip **11** (22), 3742-3751 (2011).
95. H. Bruus, Lab Chip **12** (6), 1014-1021 (2012).
96. J. Dual and T. Schwarz, Lab Chip **12** (2), 244-252 (2012).
97. J. Dual, P. Hahn, I. Leibacher, D. Moller and T. Schwarz, Lab Chip **12** (5), 852-862 (2012).
98. A. Lenshof, M. Evander, T. Laurell and J. Nilsson, Lab Chip **12** (4), 684-695 (2012).
99. A. Lenshof, C. Magnusson and T. Laurell, Lab Chip **12** (7), 1210-1223 (2012).
100. H. Bruus, Lab Chip **12** (9), 1578-1586 (2012).
101. P. Augustsson and T. Laurell, Lab Chip **12** (10), 1742-1752 (2012).
102. M. Wiklund, Lab Chip **12** (24), 5283-5283 (2012).
103. S. S. Sadhal, Lab Chip **12** (13), 2292-2300 (2012).
104. S. S. Sadhal, Lab Chip **12** (16), 2771-2781 (2012).
105. M. Gedge and M. Hill, Lab Chip **12** (17), 2998-3007 (2012).
106. M. Wiklund, H. Brismar and B. Onfelt, Lab Chip **12** (18), 3221-3234 (2012).
107. J. Dual, P. Hahn, I. Leibacher, D. Moller, T. Schwarz and J. T. Wang, Lab Chip **12** (20), 4010-4021 (2012).
108. M. Evander and J. Nilsson, Lab Chip **12** (22), 4667-4676 (2012).
109. M. Wiklund, S. Radel and J. J. Hawkes, Lab Chip **13** (1), 25-39 (2013).
110. J. J. Hawkes and S. Radel, Lab Chip **13** (4), 610-627 (2013).
111. P. Glynne-Jones and M. Hill, Lab Chip **13** (6), 1003-1010 (2013).
112. H. Bruus, Lab Chip **12** (1), 20-28 (2012).
113. J. Friend and L. Y. Yeo, Rev Mod Phys **83** (2), 647-704 (2011).
114. M. Evander, *Cell and Particle Trapping in Microfluidic Systems using Ultrasonic Standing Waves*. (Doctoral Thesis, Lund University, ISBN: 978-91-628-7525-1, 2008).
115. O. Manneberg, *Multidimensional ultrasonic standing wave manipulation in microfluidic chips*. (Doctoral Thesis, KTH, ISBN: 978-91-7415-398-9, 2009).
116. J. Beech, *Microfluidics Separation and Analysis of Biological Particles*. (Doctoral Thesis, Lund University, ISBN: 978-91-7473-195-8, 2011).
117. P. Augustsson, *On microchannel acoustophoresis-Experimental considerations and life science applications*. (Doctoral Thesis, Lund University, ISBN: 978-91-7473-202-3, 2011).
118. H. Bruus, *Theoretical microfluidics*. (Oxford University Press, 2008).
119. N.-T. Nguyen and S. T. Wereley, *Fundamentals and applications of microfluidics*. (Artech House, 2002).
120. R. S. Cobbold, *Foundations of biomedical ultrasound*. (Oxford University Press, USA, 2007).

121. N. Peekhaus and T. Conway, J Bacteriol **180** (14), 3495-3502 (1998).
122. S. M. Finegold, V. L. Sutter and G. Mathisen, in *Human intestinal microffora in health and disease* (Academic Press, New York, NY, USA, 1983), pp. 1-31.
123. M. Hill, Role of gut bacteria in human toxicology and pharmacology, 3-17 (1995).
124. C. L. Sears, Anaerobe **11** (5), 247-251 (2005).
125. L. V. Hooper and J. I. Gordon, Science **292** (5519), 1115-1118 (2001).
126. F. S. Collins, E. S. Lander, J. Rogers, R. H. Waterston and I. H. G. S. Conso, Nature **431** (7011), 931-945 (2004).
127. R. Milo, P. Jorgensen, U. Moran, G. Weber and M. Springer, Nucleic Acids Res **38**, D750-D753 (2010).
128. D. Bray, *Cell movements: from molecules to motility*. (Garland Science, 2001).
129. M. Settnes and H. Bruus, Phys Rev E **85** (1) (2012).
130. D. R. Lide, *CRC handbook of chemistry and physics*. (CRC press, 2004).
131. S. M. Hagsater, T. G. Jensen, H. Bruus and J. P. Kutter, Lab Chip **7** (10), 1336-1344 (2007).
132. R. Barnkob, P. Augustsson, T. Laurell and H. Bruus, Lab Chip **10** (5), 563-570 (2010).
133. P. Augustsson, R. Barnkob, S. T. Wereley, H. Bruus and T. Laurell, Lab Chip **11** (24), 4152-4164 (2011).
134. P. B. Muller, M. Rossi, A. G. Marin, R. Barnkob, P. Augustsson, T. Laurell, C. J. Kahler and H. Bruus, Phys Rev E **88** (2) (2013).
135. M. A. H. Weiser and R. E. Apfel, J Acoust Soc Am **71** (5), 1261-1268 (1982).
136. R. Barnkob, P. Augustsson, C. Magnusson, H. Lilja, T. Laurell and H. Bruus, in *Proc. 15th Int. Conference on Miniaturized Systems for Chemistry and Life Sciences* (The Chemical and Biological Microsystems Society, Seattle, WA, USA, 2011), pp. 127-129.
137. D. Hartono, Y. Liu, P. L. Tan, X. Y. S. Then, L. Y. L. Yung and K. M. Lim, Lab Chip **11** (23), 4072-4080 (2011).
138. D. Rabaud, P. Thibault, M. Mathieu and P. Marmottant, Phys Rev Lett **106** (13) (2011).
139. C. Eckart, Physical Review **73** (1), 68-76 (1948).
140. L. Rayleigh, Philosophical Transactions of the Royal Society of London **175**, 1-21 (1884).
141. H. Schlichting, Physikalische Zeitschrift **33**, 327-335 (1932).
142. J. F. Spengler, M. Jekel, K. T. Christensen, R. J. Adrian, J. J. Hawkes and W. T. Coakley, Bioseparation **9** (6), 329-341 (2000).
143. L. A. Kuznetsova and W. T. Coakley, J Acoust Soc Am **116** (4), 1956-1966 (2004).
144. J. J. Lei, P. Glynne-Jones and M. Hill, Lab Chip **13** (11), 2133-2143 (2013).
145. R. Barnkob, P. Augustsson, T. Laurell and H. Bruus, in *Proc. 14th Int. Conference on Miniaturized Systems for Chemistry and Life Sciences* (The Chemical and Biological Microsystems Society, Groningen, Holland, 2010), pp. 1247-1249.
146. Ferroperm Piezoceramics A/S. (2003). *Ferroperm Piezoceramics High Quality Components and Materials for the Electronics Industry* [Catalogue]. Kvistgaard, Denmark: Author.
147. H. J. Dong, J. Wu, G. Y. Zhang and H. F. Wu, Ieee T Ultrason Ferr **59** (2), 205-210 (2012).
148. Y. Mizutani, T. Suzuki, H. Ikeda and H. Yoshida, Ieee Ind Elec, 983-986 (1996).
149. N.-G. Holmer and K. Lindström, *New Methods in Medical Ultrasound*. (Lund Institute of Technology/Malmö General Hospital, LUTEDX/(TEEM-1001)/1-420/(1978), 1978).
150. L.-S. Jang, S.-H. Chao, M. R. Holl and D. R. Meldrum, Sensors and Actuators A: Physical **138** (1), 179-186 (2007).

151. O. Manneberg, B. Vanherberghen, B. Onfelt and M. Wiklund, Lab Chip **9** (6), 833-837 (2009).
152. A. Nilsson, F. Petersson, H. Jonsson and T. Laurell, Lab Chip **4** (2), 131-135 (2004).
153. M. Evander, A. Lenshof, T. Laurell and J. Nilsson, Anal Chem **80** (13), 5178-5185 (2008).
154. M. Evander and M. Tenje, J Micromech Microeng **24** (2), 027003 (2014).
155. M. Groschl, Acustica **84** (3), 432-447 (1998).
156. J. Kaitila, M. Ylilammi, J. Ella and R. Aigner, Ultrason, 84-87 (2003).
157. R. Thalhammer and R. Aigner, Ieee Mtt-S, 225-228 (2005).
158. J. A. Brown, E. S. Foster, A. Needles, E. Cherin and G. R. Lockwood, Ieee T Ultrason Ferr **54** (9), 1888-1894 (2007).
159. K. Yamaguchi, S. Sano, N. Seki and M. Imamoto, *Linear array ultrasonic transducer*. (Patent: US4385255 A, 1983).
160. M. Almqvist, M. Torndahl, M. Nilsson and T. Lilliehorn, Ieee T Ultrason Ferr **52** (12), 2298-2302 (2005).
161. J. V. Norris, M. Evander, K. M. Horsman-Hall, J. Nilsson, T. Laurell and J. P. Landers, Anal Chem **81** (15), 6089-6095 (2009).
162. J. F. Spengler, W. T. Coakley and K. T. Christensen, Aiche J **49** (11), 2773-2782 (2003).
163. S. Ekstrom, L. Wallman, D. Hok, G. Marko-Varga and T. Laurell, J Proteome Res **5** (5), 1071-1081 (2006).
164. D. Nedelkov, D. A. Phillips, K. A. Tubbs and R. W. Nelson, Mol Cell Proteomics **6** (7), 1183-1187 (2007).
165. D. Nedelkov, Proteomics **8** (4), 779-786 (2008).
166. A. G. Madian, N. S. Rochelle and F. E. Regnier, Anal Chem (2012).
167. K. Sparbier, T. Wenzel, H. Dihazi, S. Blaschke, G. A. Muller, A. Deelder, T. Flad and M. Kostrzewa, Proteomics **9** (6), 1442-1450 (2009).
168. N. L. Anderson and N. G. Anderson, Molecular & cellular proteomics : MCP **1** (11), 845-867 (2002).
169. N. L. Anderson, N. G. Anderson, T. W. Pearson, C. H. Borchers, A. G. Paulovich, S. D. Patterson, M. Gillette, R. Aebersold and S. A. Carr, Mol Cell Proteomics **8** (5), 883-886 (2009).
170. F. G. Strathmann and A. N. Hoofnagle, Am J Clin Pathol **136** (4), 609-616 (2011).
171. L. H. Cazares, D. A. Troyer, B. Wang, R. R. Drake and O. J. Semmes, Anal Bioanal Chem **401** (1), 17-27 (2011).
172. B. Hammarström, T. Laurell, M. Evander, J. Nilsson and S. Ekström, in *Proc. 13th Int. Conference on Miniaturized Systems for Chemistry and Life Sciences* (The Chemical and Biological Microsystems Society, Jeju, Korea, 2009), pp. 1344-1346.
173. V. Havlicek, K. Lemr and K. A. Schug, Anal Chem **85** (2), 790-797 (2013).
174. D. Martiny, A. Dediste and O. Vandenberg, Eur J Clin Microbiol **31** (9), 2269-2281 (2012).
175. Bruker Daltronik GmbH. (August 2013). *MALDI Sepsityper Kit – Instructions for Use (Revision 2)* [Brochure], Bremen, Germany: Author.